Journal of Power, Energy, and Control

Research article

Time Delay Compensation for the Superheated Steam Temperature Control System Based on a Practical Feedforward Gain-Scheduling Cascade Control Design with Stability Analysis

Tahereh Gholaminejad[1,2]*, Fereshteh Dadkhah-Tehrani[1], Mohsen Maboodi[1]

[1] Digitalization Department, Mapna Electric and Control, Engineering and Manufacturing Company (MECO), Karaj, Iran
[2] Department of Electrical Engineering, K. N. Toosi University of Technology, Tehran, Iran
*Correspondence: gholaminejad.tahereh@mapnaec.com

https://doi.org/10.62777/pec.v2i2.46

Received: 5 January 2025
Revised: 20 September 2025
Accepted: 2 October 2025
Published: 4 October 2025

Abstract: Controlling the temperature of superheated steam (SST) is essential for the safe and efficient operation of combined cycle power plants, but it has become challenging due to frequent load variations and safety requirements. Traditional PI controllers may struggle to provide optimal performance because of non-linearity, time delays, and disturbances, particularly under wide-range load conditions. This paper proposes a new feedforward gain-scheduling cascade control strategy that compensates for time delays while ensuring stable SST without complicating the control system. The method incorporates a well-defined feedforward control mechanism into a gain-scheduling PI structure, enabling quick adjustments of the water spray control valve to prevent SST overshoots during sudden power fluctuations. A stability analysis is included, and the proposed strategy has been successfully simulated and implemented at two real combined cycle power plants in Iran, demonstrating its effectiveness in maintaining smooth temperature control and enhancing power output without adding complexity to the system.

Keywords: superheated steam temperature, gain-scheduling control, feedforward control, particle swarm optimization, power increment

1. Introduction

As the demand for power continues to rise, managing power plants becomes increasingly challenging. Experts predict that global net generation will grow by 2.2% annually until 2040 [1]. Controlling superheated steam temperature (SST) is essential for the safe and cost-effective operation of combined cycle power plants. The ability to adapt to fluctuating power plant load demands heavily relies on the performance of superheater control loops. If the SST exceeds its upper limit, it can damage the superheater and high-pressure (HP) components of the steam pipelines. Conversely, if the SST falls below its lower limit, power generation efficiency may decline, adversely affecting the economical operation of the combined cycle power plants. Even a brief period with steam temperature above the specified limit can cause irreparable damage to the boiler's metal tubes and lead to unscheduled boiler shutdowns. Low superheated

steam temperatures can result in water droplet formation, which can severely damage turbine blades and reduce boiler efficiency. Frequent fluctuations in superheater temperature can impose thermal stresses, leading to premature failures of metal pipes. Consequently, most researchers recommend maintaining SST within ±5 °C of its set-point to ensure the safe and efficient operation of power plant units [2].

Conventional Proportional-Integral (PI) cascade control faces challenges in ensuring satisfactory control performance during wide load variations due to process model nonlinearity, multi-source disturbances, and the limitations of the PI controller [2]. This issue is particularly evident in wide-range load regulation. To address these challenges, many improved and advanced control strategies have been developed, including neuro-Proportional-Integral-Differential (neuro-PID) [3], Internal Model Control (IMC) [4], Fractional-Order PID (FOPID) control [5], nonlinear control strategies [6], [7], multivariable constrained predictive control [8], Model Predictive Control (MPC) [9], [10], neural networks [11], fuzzy logic control [12], fuzzy model predictive control [13], Dynamic Matrix Control (DMC) [14], neuro-fuzzy Generalized Predictive Control (GPC) [15], predictive feed-forward control [16], and the Active Disturbance Rejection Controller (ADRC) [1], [2], [17], [18], [19]. Additionally, robust PID controllers based on data-driven feedback compensation methods have been explored in [20], yielding better control performance than the original PID controller.

Although these control strategies have shown positive results in numerical simulations, they are rarely implemented in practical units due to their high computational complexity, which renders them unsuitable for deployment in distributed control system (DCS) function blocks. Furthermore, some control strategies rely heavily on an exact mathematical model of the superheater, which is difficult to achieve and varies with working conditions. In fact, the superheater system model can change significantly with load variations. Therefore, the superheater temperature control system must be robust enough to manage the modeling uncertainties caused by these load fluctuations. For instance, a study in [21] presents a Long Short-Term Memory (LSTM) model to obtain a model and a MPC controller for the SST control loop, which effectively captures the time delay, multivariable coupling, and nonlinear dynamics of steam temperatures. However, as noted, the application of advanced control strategies such as MPC in DCS environments is typically not feasible. On the other hand, due to non-linearity and time delay in the SST process behavior and various disturbances, the traditional PI controller with fixed parameters in a cascade control strategy for the SST may not guarantee optimal control performance, especially in wide-range load regulation conditions. In fact, when using a cascade control loop for the SST control with the fixed parameters PI controllers (the structure that is now pervasive in practice), it is observed that there is a significant time delay between the change in the load increment and the opening of the spray valve. This delay can cause the SST to rise too much, which could trigger an alarm or trip that forces the power plant operator to reduce the set-point in order to control temperature during these emergency conditions. This reduction in set-point will consequently cause a loss in the steam turbine produced power. So, a method that can compensate for this time delay while maintaining a smooth SST without further complicating the control system is preferred.

In this paper, modifications to the current control logic of the SST loop are proposed to compensate for the mentioned time delay and eliminate temperature overshoot. The proposed method is based on improving the existing PI-based cascade control system by adding a well-defined feedforward controller and using a gain-scheduling PI feedback controller instead of the current PI feedback controller. The most

important feature of the proposed method is its ability to be implemented in the power plant DCS without increasing the cost in comparison to the existing control system while can effectively address the critical issue of controlling SST in power plants and also enhance the power output of a steam cycle. The advantages of the proposed structure in this paper are as follows:

- Reduction of SST overshoots during extreme changes in gas turbine power, flue gas temperature, or duct burner fuel flow.
- The possibility of increasing the SST set-point (from the current value of 517 or 518 °C to higher values, e.g., 523 °C) and consequently increasing the power produced.
- Reduction of water spray control valve fluctuations.
- Because PI controllers are used, this structure can be easily implemented without increasing the complexity of the DCS system.
- By using feedforward control, disturbances are eliminated before they enter the outer loop.
- The use of feedforward control reduces the delay between the spray control valve and changes in load.
- With the implementation of a gain-scheduling structure, the PI controller coefficients adjust to faster values during significant fluctuations in the system.
- By implementing optimization-based tuning methods, accurate coefficients for the PI controllers are obtained.
- The stability analysis and the stability margin for the proposed controller are presented.

The paper is structured as follows. The next section provides a brief introduction to the SST process, its model identification and the regular cascade control strategy. In Section 3, the proposed feedforward gain-scheduling cascade control structure is introduced. Section 4 presents a tuning procedure based on the particle swarm optimization (PSO) method and illustrates the control performance of the proposed structure through numerical simulation on the identified model of the SST control system. In Section 5, the stability analysis and the stability margin for the proposed controller are presented. In Section 6, at first, the result of implementing the proposed control structure in unit 1 Heat Recovery Steam Generator (HRSG) of 968MW Pareh-Sar combined cycle power plant is being investigated. Since duct burners have a great effect on the SST, it is necessary to consider the control of the SST loop in 2 states of the duct burner being on and off. Due to the fact that the duct burners in Pareh-Sar power plant are always turned off due to operational reasons, the effect of the burner on the SST control loop is investigated on the unit 4 HRSG of 942MW Parand power plant. The paper conclusion is finally presented in section 7.

2. SST Process Description and Model Identification

2.1. SST Process Description

In an HRSG, the saturated and dried steam exits from the top of the HP drum and enters the HP superheater section (the closest section to the gas turbine exhaust), and after passing through the two stages of the superheater harp tubes, the steam is passed through a so called de-superheater, which controls steam temperature by spraying water. Then, the steam enters the third stage of the superheater harp tubes and finally, superheated steam is produced with a temperature around the set-point. An image of the superheated steam temperature control loop can be seen in Figure 1. In some HRSGs, the superheater is divided into 3 stages: 1st, 2nd, and 3rd superheaters, and the de-

superheater is installed between the 2nd stage and 3rd stage superheaters. Next, the superheated steam is sent to the steam turbine. The increase in temperature of superheated steam is not linear. Therefore, there is a need for a well-designed control system for these nonlinear temperature changes. De-superheaters can achieve this goal with a cascade PI control structure.

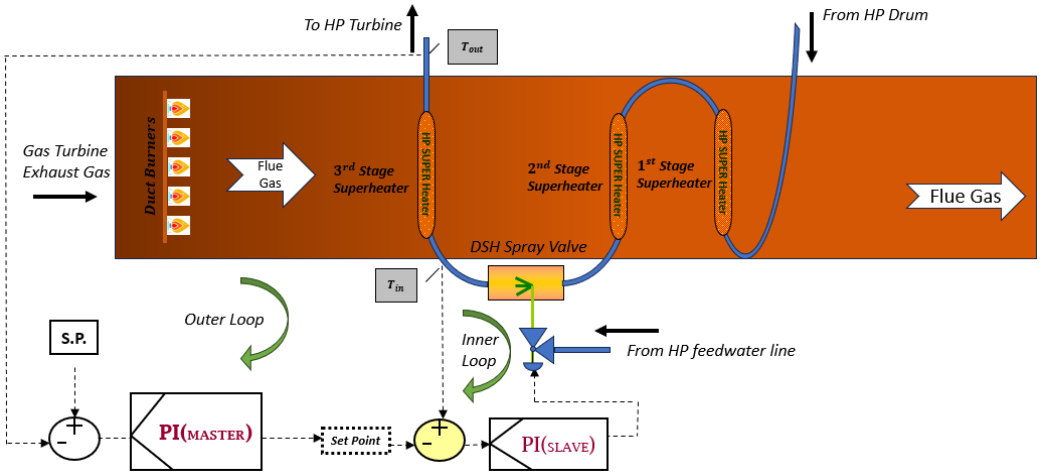

Figure 1. Schematic diagram of the power plant superheater with a cascade control system.

In order to control the SST, the temperature measured in the HP superheater steam line is compared with the designed SST set-point of 523°C. Then, the amount of water needed to spray the superheater steam is adjusted to limit the temperature of the superheater steam. According to Figure 1, this control loop consists of 2 inner (secondary or slave) and outer (primary or master) cascade loops. The manipulated variable is the position of the water spray control valve to cool the superheated steam at the outlet of the 3rd stage superheater. The cooling water is taken from an intermediate stage of the HP boiler feed pump (BFP). According to the process type, the secondary steam temperature T_{in} responds to rapid water spray changes, so the PI controller is considered as the secondary controller to deal with the inner loop disturbances. However, the outer loop variable T_{out} due to the helical harp tubes is a slow process with various disturbances, which makes it difficult to design a suitable controller. The primary controller forms another set-point by comparing the output steam temperature from the last stage of the superheater T_{out} with the SST set-point (523°C). In fact, the control signal of the primary controller forms the set-point of the slave controller, and based on the comparison of this new set-point with the temperature of the steam entering the last stage of the superheater, the control signal of the secondary controller is created to command the water spray control valve to superheat steam. However, due to the inefficient structure currently present in the power plants, the set-point is adjusted to values lower than the designed set-point of 523°C (e.g., 515°C). This requirement would result in a significant loss of power, affected by the limitation in the existing control structure. By using the method proposed in this article, we will show that the set-point can be set to its initial design value of 523°C.

2.2. SST Model Identification

Figure 2 shows the cascade control loop block diagram of the SST control system. As it is seen, the SST control system is constructed by the two linear transfer function models: $G_{p_s}(s)$ and $G_{p_m}(s)$. The inner loop transfer function model $G_{p_s}(s)$ represents the relation between the water spray valve position input and the desuperheater outlet temperature output, while the outer loop transfer function model $G_{p_m}(s)$ represents the

relation between the desuperheater outlet temperature input and the superheater outlet temperature output. The manipulated variable is the water spray valve position, which is the output of the inner loop controller $G_{c_s}(s)$ or $PI_s(s)$ denoted as u_{in}. The SST set-point $S.P.$ is the expected outlet temperature of the 3rd stage superheater, and the output of the outer loop controller $G_{c_m}(s)$ or $PI_m(s)$, which is denoted as u_{out}, is the set-point of the inner loop. The SST system is subject to multi-source disturbances such as gas turbine load demand, HP superheated steam flow, and duct burner fuel flow. The system's complexity makes it challenging to build an accurate mathematical model. Therefore, the SST control system's controller must possess a strong ability to reject disturbances while maintaining desired robustness and independence from a strict mathematical model.

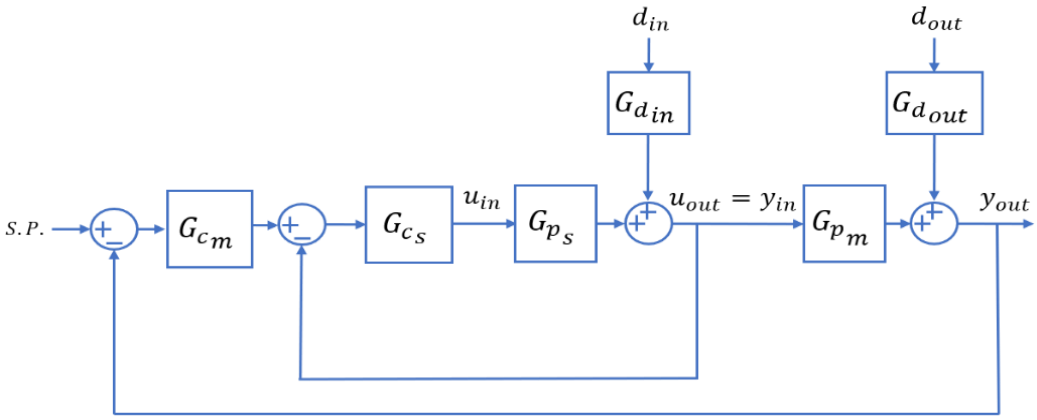

Figure 2. General block diagram of SST cascade control system.

The input-output-disturbance signals for the inner and outer loops are defined in Table 1. These signals have been selected with consideration of the inner and outer loops process concepts, and with the goal of achieving the best achievable fitness between the output signals of the inner and outer loops with the actual measured signals. In this paper, identifying the SST inner and outer loop models along with the disturbances affecting them is done according to the following points:

- Identification is done according to the closed-loop measured real data (closed-loop identification)
- In order to reduce the complexity as much as possible, the minimum degree identification is performed for the transfer functions. In this paper, transfer functions are considered as 2nd order.
- The identification methods based on prediction error minimization, such as least square regression, are used. In this paper, the autoregressive with an exogenous input (ARX) model is considered.

Since the process transfer function shows the ratio of the output changes to the input changes, the average of each signal is subtracted from that signal before identification (detrending).

Table 1. Defining input, output, and disturbances for SST inner and outer control loops.

	Output	Input	Disturbances
Inner Loop	y_{in}: desuperheater outlet temperature (T_{in})	u_{in}: water spray valve position	D_{in1}: inlet steam temperature D_{in2}: steam flow rate
Outer Loop	y_{out}: superheater outlet temperature (T_{out})	U_{out}: desuperheater outlet temperature ($U_{out} = y_{in}$)	D_{out1}: gas turbine exhaust temperature D_{out2}: steam flow rate D_{out3}: gas turbine power D_{out4}: duct burner fuel flow

For a 2-hour interval of measured data on 30-April-2023 from Pareh-Sar combined cycle power plant, and a 3-hour interval of measured data on 23-July-2024 from Parand combined cycle power plant, the transfer functions for the inner plant model and its disturbances, as well as the transfer functions for the outer plant model and its disturbances, are obtained in Equation (1) to (15).

Pareh-Sar SST model identification:

$$G_{p_{in}} = \frac{0.0003737\,\mathrm{s} - 3.54e^{-6}}{s^2 + 0.06334\,\mathrm{s} + 0.000689} \tag{1}$$

$$G_{d1_{in}} = \frac{0.0336\,\mathrm{s} + 0.0003041}{s^2 + 0.06334\,\mathrm{s} + 0.000689} \tag{2}$$

$$G_{d2_{in}} = \frac{-0.007344\,\mathrm{s} - 0.0003184}{s^2 + 0.06334\,\mathrm{s} + 0.000689} \tag{3}$$

$$G_{p_{out}} = \frac{-0.006987\,\mathrm{s} + 0.000353}{s^2 + 0.06706\,\mathrm{s} + 0.000687} \tag{4}$$

$$G_{d1_{out}} = \frac{-0.006239\,\mathrm{s} + 0.000476}{s^2 + 0.06706\,\mathrm{s} + 0.000687} \tag{5}$$

$$G_{d2_{out}} = \frac{0.002024\,\mathrm{s} - 0.0005043}{s^2 + 0.06706\,\mathrm{s} + 0.000687} \tag{6}$$

$$G_{d3_{out}} = \frac{9.982e^{-6}\,\mathrm{s} + 5.153e^{-7}}{s^2 + 0.06706\,\mathrm{s} + 0.0006875} \tag{7}$$

Parand SST model identification:

$$G_{p_{in}} = \frac{4.725e^{-5}\mathrm{s} - 9.805e^{-6}}{s^2 + 0.1393\,\mathrm{s} + 0.002254} \tag{8}$$

$$G_{d1_{in}} = \frac{-0.0322\,\mathrm{s} + 0.0023581}{s^2 + 0.1393\,\mathrm{s} + 0.002254} \tag{9}$$

$$G_{d2_{in}} = \frac{-0.0322\,\mathrm{s} + 0.002358}{s^2 + 0.1393\,\mathrm{s} + 0.002254} \tag{10}$$

$$G_{p_{out}} = \frac{-0.004535\,\mathrm{s} + 0.0003348}{s^2 + 0.1135\,\mathrm{s} + 0.001266} \tag{11}$$

$$G_{d1_{out}} = \frac{0.002011\mathrm{s} + 0.0004244}{s^2 + 0.1135\,\mathrm{s} + 0.001266} \tag{12}$$

$$G_{d2_{out}} = \frac{0.01343\,\mathrm{s} - 0.0005208}{s^2 + 0.1135\,\mathrm{s} + 0.001266} \tag{13}$$

$$G_{d3_{out}} = \frac{-6.822e^{-5}\,\mathrm{s} + 4.451e^{-5}}{s^2 + 0.1135\,\mathrm{s} + 0.001266} \tag{14}$$

$$G_{d4_{out}} = \frac{0.005179\,\mathrm{s} + 0.0002735}{s^2 + 0.1135\,\mathrm{s} + 0.001266} \tag{15}$$

Since the duct burner is turned off in the Pareh-Sar power plant, the transfer function G_{d4out} is not considered for it. Figure 3 shows the real measured and the modeled outputs of the inner and outer loops for the Pareh-Sar power plant. As can be seen, the identification results for both loops are acceptable.

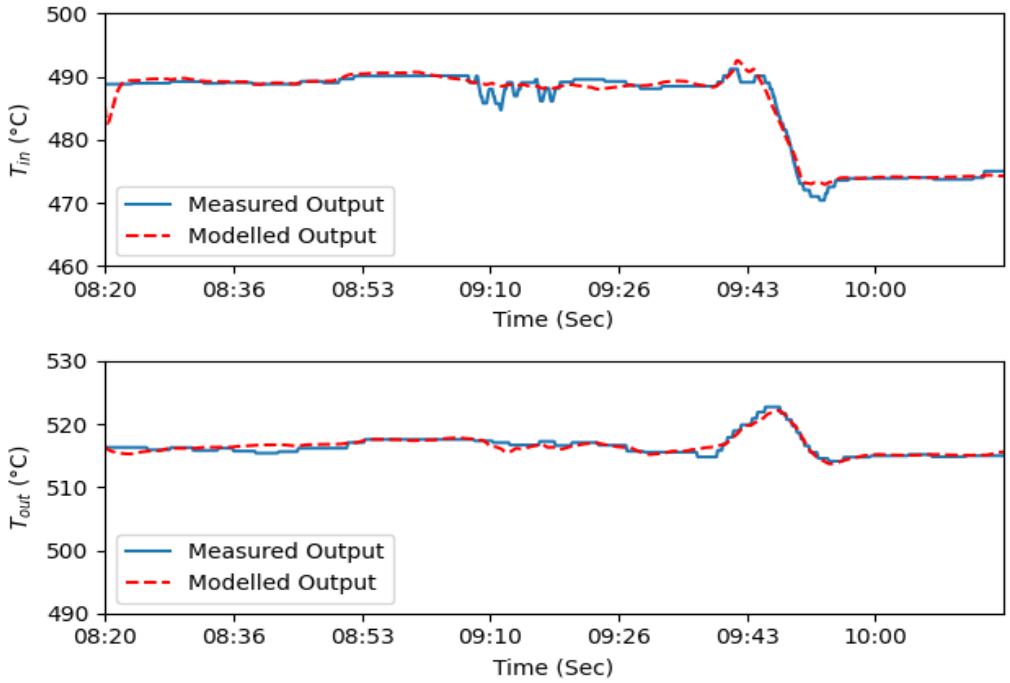

Figure 3. Identification result for inner and outer loop model outputs of the SST control system for a 2-hour interval of measured data on 30 April 2023 from Pareh-Sar combined cycle power plant.

3. SST Control Loop Design

3.1. Motivation

As previously mentioned, due to overshoots in SST, real data shows that the selected SST set-point in many power plants is often set around 512°C to 517°C, while the designed SST set-point is 523°C. This difference can lead to a significant loss of power. Reducing temperature fluctuations can allow for an increase in the set-point, resulting in higher superheated steam temperature and increased power production. Therefore, it is desirable to minimize superheater temperature fluctuations and keep the error at or near zero. As mentioned, the cause of the overshoots in SST is the time delay in this system. To maintain the superheater temperature as constant as possible and compensate for the described delay, this paper proposes a feedforward cascade gain-scheduling PI control structure, which is explained in the next section.

3.2. Proposed Feedforward Gain-Scheduling Cascade Control

The block diagram of the proposed feedforward cascade gain-scheduling control is presented in Figure 4. The specified signals in this figure are defined in Table 2. In the following sections, details of the constituent functions in the block diagram of Figure 4 are described.

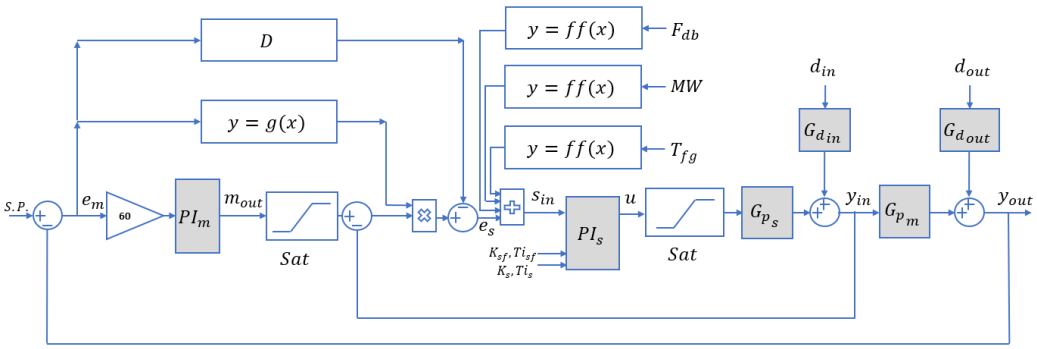

Figure 4. Block diagram of the proposed feedforward gain-scheduling cascade control.

Table 2. SST block diagram signals definitions.

Signal	Description
e_m	Master loop error
m_{out}	Master controller output ≡ slave loop set-point
e_s	Slave loop error
s_{in}	Slave controller input
$u = s_{out}$	Slave controller output ≡ loop control signal
y_{in}	Inner loop output
y_{out}	Outer loop ouput
d_{in}	Inner loop disturbance
d_{out}	Outer loop disturbance
$S.P$	Outer loop set-point (SST set-point)

3.2.1. Feedforward Function in the SST Control Logic

In combined cycle power plants, when the gas turbine load increases, the SST also rises; however, there is a significant time delay between the change in load and the opening of the spray valve. Such a delay is also seen during changes in the fuel flow of the duct burner (with a lower amount than the delay related to load changes). This delay causes the SST to rise excessively. In this context, it is possible to compensate for this time delay and eliminate temperature overshoot by modifying the control logic of this loop. Considering that the HRSG has a time delay compared to the gas turbine, all the signals involved in the SST cascade control loop will respond to changes in gas turbine load with a delay. Therefore, to enable the HP steam to respond to changes in load demand promptly, and for the water spray valve to react quickly during significant changes in the temperature of the gas turbine exhaust, signals related to the gas turbine such as gas turbine fuel flow rate, gas turbine power, and signals related to the duct burner, like duct burner fuel flow rate or gas turbine exhaust gas temperature can be utilized to manipulate the spray valve position.

In this paper, Equation (16) is designed to construct a feedforward control signal from an input signal $x(t)$.

$$F(X(s)) = X(s) - \frac{1}{180s + 1}X(s) \tag{16}$$

where $F(X(s))$ is the Laplacian transform of the feedforward function $f(x(t))$, $x(t)$ is used for the selected disturbances as the gas turbine power $MW(t)$, the flue gas temperature (the temperature of the HRSG flue gas just before it passes through the HP superheater harps) $T_{fg}(t)$, and the duct burner fuel flow $F_{db}(t)$. According to Equation (16), the function $f(x(t))$ calculates the difference between the signal x at the current time and the signal x in 3 minutes prior to it (the time delay 180 seconds), so that in case of significant changes in the signal x during these 3 minutes, a feedforward signal $ff(x(t))$ will be sent to the water spray control valve to open. In order to limit the operation area of the feedforward signal, the value of $ff(x(t))$ is saturated to an upper limit (UL). So, the function $y = ff(x)$ in Figure 4 is defined as follows:

$$ff\big(x(t)\big) = \begin{cases} f(x(t)) & if \quad f(x(t)) \le UL \\ UL & if \quad UL \le f(x(t)) \end{cases} \tag{17}$$

where, the value of UL should be specifically set according to the conditions and requirements of each power plant. By adding the $ff\big(x(t)\big)$ feedforward signals for the

gas turbine power $MW(t)$, the flue gas temperature $T_{fg}(t)$, and the duct burner fuel flow $F_{db}(t)$, the error of the inner (slave) loop is defined as follows:

$$s_{in}(t) = K_{ff\_mw} \times ff\big(MW(t)\big) + K_{ff\_t} \times ff\left(T_{fg}(t)\right) + K_{ff\_db} \times ff\big(F_{db}(t)\big) + e_s(t) \quad (18)$$

where, K_{ff_mw}, K_{ff_t} and K_{ff_db} are the gas turbine power, the flue gas temperature, and the duct burner fuel flow feedforward signal's gains, respectively.

Remark 1: Selecting the threshold limit (UL) for the designed feedforward signals added to the inner loop deviation causes these signals to saturate out of range. In this way, the amount of manipulation in the inner loop control signal is always within a limited range. Not limiting the feedforward signal can result in temperature overshoot or undershoot during rapid changes in gas turbine power or fuel duct burner flow.

Remark 2: In Equation (18), each of the $ff(x(t))$ signals is added to the inner loop error with a different coefficient. These coefficients, in addition to uniting the feedforward signals of different types (temperature, flow rate, etc.), show the contribution of each signal in improving the error signal to better control the temperature. Therefore, they will be set based on the importance of each feedforward signal and may differ for each power plant unit according to its requirements. It should be noted that since the flue gas temperature $T_{fg}(t)$ has a time delay compared to the gas turbine power signal $MW(t)$, the feedforward signal composed of the $MW(t)$ has a greater ability to speed up the opening of the water spray valve and so has more effect than the feedforward signal composed of the flue gas temperature signal $T_{fg}(t)$. Therefore, a larger coefficient should be considered for it. These coefficients will be computed for Pareh-Sar power plant at section 4.

Remark 3: In HRSG systems, a duct burner can be used to create additional combustion using the oxygen available in the exhaust gases from the gas turbine to increase the steam cycle production, provide greater flexibility, and achieve higher thermal efficiency. Therefore, when there is a need for increased power generation, the duct burners are turned on. The changes in the fuel flow in a duct burner are made based on the HP steam flow. This means that when the duct burner is on, if the HP steam flow of the HRSGs increases, the fuel flow of the duct burner needs to be decreased in order to moderate the HP steam temperature, and vice versa. Therefore, changes in the duct burner fuel flow lead to changes in the exhaust gas temperature inside the HRSG, and thus affect the water spray control valve opening or closing. It can be shown that the changes in the water spray control valve position relative to the duct burner fuel flow have a time delay. Therefore, the duct burner fuel flow is also considered as a feedforward signal.

3.2.2. PI Controllers Block

In the SST control logic, with the aim of achieving a desired performance by using the simplest available controllers, PI controllers with the following definitions are used:

$$PI_m(s) = K_m\left(1 + \frac{1}{Ti_m s}\right)$$
$$PI_s(s) = K_s\left(1 + \frac{1}{Ti_s s}\right) \quad (19)$$

where, PI_m and PI_s are the master and slave PI controllers, respectively and K and Ti are the PI controller parameters. On the other hand, as it was said, this loop does not perform properly using the PI controllers with fixed parameters. In this paper, it is shown that only by changing the slave PI parameters, the performance of the SST control loop can be significantly improved. The gain-scheduling PI in inner loop is defined according to the

designed feedforward signal $ff(x(t))$. In such a way that, if magnitude of the feedforward signal $ff(x(t))$ is above a lower threshold limit TRS, the slave controller parameters will switch over to faster parametes (larger K_s and smaller Ti_s named as K_{sf} and Ti_{sf}). The activation condition for the inner loop gain-scheduling PI is defined as follows:

$$gain\_sch\_act(x(t)) = \begin{cases} 0, & if\ \ abs(ff(x(t))) < TRS \\ 1, & if\ \ abs(ff(x(t))) \geq TRS \end{cases} \tag{20}$$

The value of TRS shall be specifically set according to the conditions and requirements of each power plant.

Figure 5 shows the gas turbine power signal $x(t) = MW(t)$, its corresponding feedforward signal $ff(MW(t))$ and also the corresponding gain-scheduling activation signal $gain\_sch\_act(x(t))$. In fact, by applying the gain-scheduling PI controller, in addition to adding the feedforward signal that accumulates with the inner loop error e_s, when the changes in the gas turbine power signal are extreme, the parameters of the inner PI controller also change. So, the inner loop PI controller in (19) can be rewritten as follows:

$$PI_s(s) = \begin{cases} K_s\left(1 + \dfrac{1}{Ti_s s}\right), & if\ \ gain\_sch\_act(x(t)) = 0 \\ K_{sf}\left(1 + \dfrac{1}{Ti_{sf} s}\right), & if\ \ gain\_sch\_act(x(t)) = 1 \end{cases} \tag{21}$$

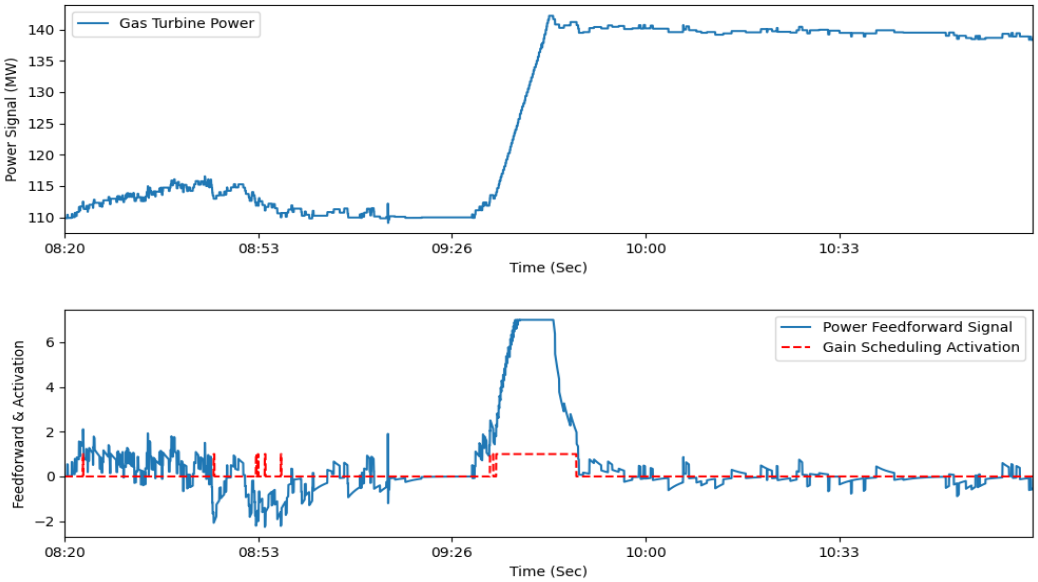

Figure 5. Gas turbine power signal. Its feedforward signal and the gain-scheduling activation signal for a measured data on 30-April-2023 from Pareh-Sar.

3.2.3. Block Function g

The $y = g(x)$ block in the SST control loop in Figure 4 is used to connect the master loop error to the slave loop error. It is a function of the master loop absolute error that is multiplied by the slave loop error (as a variable gain). This function is actually a "look up table function" which is designed as Table 3, where $abs(x)$ is the absolute value of the signal x.

Table 3. *y = g(x)* function detail.

abs(x)	*y*
0	10
0.5	10
1	20
3	50
4	100
10	130
11	130
1,000	130

According to Table 3, this block considers a coefficient for the inner loop error according to the outer loop error. By looking carefully at the values in Table 3, it can be seen that the bigger the error of the outer loop, the bigger is this coefficient and vice versa. In fact, the design logic of this table is based on the proximity to the main set-point. The further we are from the set-point, it is necessary to open or close the valve faster to reach the set-point, so we apply a larger coefficient to the inner loop. On the contrary, when we are close to the set-point, we need to slow down to avoid swings around the set-point. However, this block can also be viewed as an adaptive coefficient that is multiplied by the error of the slave loop. In fact, the existence of g helps to reach an optimal and general coefficient setting. If we remove g from the loop, to compensate for the slowness of the loop, it is necessary to choose a larger K_m coefficient and a smaller Ti_m, which may cause fluctuations in the steady-state and ultimately makes it more difficult to reach the optimal coefficients.

3.2.4. Saturation Block

In cascade control loops, a strict threshold limit has been included for the output of the master controller. In a cascade control loop, the master controller is considered as a set-point for the slave controller. Hence, the master controller's output must be satisfied a rational region. In this paper, the following relation is considered for the master controller output:

$$\begin{aligned} y_{in} - 5 < m_{out} < y_{in} + 10 \qquad & \text{if valve is open} \\ y_{in} - 5 < m_{out} < y_{in} + 20 \qquad & \text{if valve is closed} \end{aligned} \tag{22}$$

Equation (22) means that the output of the master controller is always within a range of 15 or 25 degrees around T_{in} and depending on the conditions, it may enter the upper or lower saturation limits. The *Sat* block in the inner loop also applies the upper and lower saturation limits of the control signal, which is generally necessary for any control loop. Since the control signal of the inner loop is applied to the valve control, the saturation limits are between 0 and 100%.

3.2.5. Derivative Block

In the SST control loop block diagram, both inner and outer controllers are of PI type. But a derivative function is also placed separately before the inner controller. As shown in the block diagram in Figure 4, the derivative of the outer loop error is summed with the inner loop error before entering the inner controller. D controller is defined as follows:

$$D = \frac{500s}{80s + 1} \tag{23}$$

where adding the pole in the denominator of the above relation is to make the controller causal. Using the *D* controller has a similar rationale to defining the feedforward function $ff(x(t))$. This controller intends to increase the valve opening speed and then reduce temperature peaks by adding the changes in the outer loop error to the inner loop error.

3.3. Algorithm of the Proposed Feedforward Gain-Scheduling Cascade Control Approach

Algorithm below illustrates the steps of implementing the proposed feedforward cascade gain-scheduling control:

- *Input.* Identified models of inner and outer loop systems and disturbance models (1) to (8), initial values for input, output and disturbance signals in Table 1.
- Do the following steps for $t = 1,2, \dots, T_{sim}$, where T_{sim} is the simulation time.
- *Step 1.* Compute the master error signal $e_m(t)$.
- *Step 2.* Apply the error signal $e_m(t)$ to the master controller $m_{out}(t)$.
- *Step 3.* Compute the upper and lower limitations (15) and check whether the computed $m_{out}(t)$ satisfies the limitations.
- *Step 4.* Compute the error signal $e_s(t)$ according to Fig. 4 as follows:
- $e_s(t) = \mathcal{L}^{-1}\left(\frac{500s}{80s+1} e_s(s)\right)(t) + g(e_s(t))(m_{out}(t) - y_{in}(t))$
- *Step 5.* Calculate the slave error signal $s_{in}(t)$ from (11).
- *Step 6.* If $gain\_sch\_act(MW(t))$ or $gain\_sch\_act\left(T_{fg}(t)\right)$ or $gain\_sch\_act(F_{db}(t))$ is equal to 1, $PI_s(s) = K_{sf}\left(1 + \frac{1}{Ti_{sf}s}\right)$, otherwise $PI_s(s) = K_s\left(1 + \frac{1}{Ti_s s}\right)$.
- Step 7. Apply the error signal $s_{in}(t)$ to the slave controller to compute $u(t)$.
- Step 8. If $u(t)$ is between 0% to 100%, then apply it to the inner loop system to calculate $y_{in}(t)$.
- Step 9. Apply $y_{in}(t)$ to the outer loop system to calculate $y_{out}(t)$.
- Step 10. Set $t = t + 1$ and return to Step 1.

In the next section, an analysis is presented for stability proof of the proposed control approach.

4. Stability Analysis

In this section, we conduct a thorough stability analysis of the proposed feedforward gain-scheduling cascade control illustrated in Figure 4. Figure 6 presents a modified block diagram for this control strategy. In this figure, the function $y = g(x)$ is replaced by an adaptive gain AG. As previously mentioned, this function can be interpreted as an adaptive coefficient that is multiplied by the error of the slave loop. To assess the stability of the cascade control block diagram shown in Figure 6, we propose the following lemma at first.

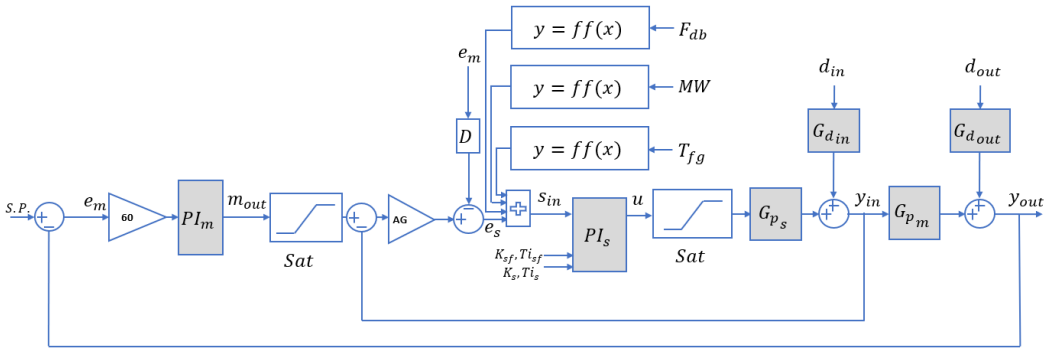

Figure 6. Block diagram of the proposed feedforward gain-scheduling cascade control.

Lemma 1. *Consider a cascade control system where both the inner and outer system models are stable. If the inner loop is internally stable and the outer loop controller is a PI controller, then a stability margin can be readily computed for the outer loop PI coefficients*.

Proof. The proof is straightforward. In a cascade control system (such as the one illustrated in Fig. 2), if the inner loop is stable, we can represent the closed-loop transfer function for the inner loop as $G_{cl_{p_{in}}}(s)$. Consequently, the characteristic equation for the cascade loop is as follows:

$$1 + G_{cl_{p_{in}}}(s)G_{p_{out}}(s)K_m\left(1 + \frac{1}{Ti_m s}\right) = 0 \tag{24}$$

where $G_{cl_{p_{in}}}(s)$ and $G_{p_{out}}(s)$ are two stable transfer functions with specific coefficients, the stability margin for the PI controller coefficients K_m and Ti_m can be easily computed using classical stability analysis methods, such as the Routh-Hurwitz criterion.

According to Lemma 1, if we can prove the stability of the inner loop control system, then the stability of the entire cascade control system is straightforwardly established. Therefore, we will focus on the stability of the inner loop system.

Figure 7 provides a modified sketch of the inner loop block diagram presented in Figure 6, which is used to analyze the internal stability of the designed feedforward-feedback control system depicted in this figure. In Figure 7, three disturbances affecting the feedback loop d_1, d_2 and d_3 are identified as internally generated signals. Let $r_{in} := Sat(m_{out})$. We also assume that the inputs $r_{in}(t)$, $d_{in}(t)$ and $e_m(t)$ are bounded signals, i.e., $r_{in}(t), d_{in}(t), e_m(t) \in \mathcal{L}_2[0,\infty)$, where $\mathcal{L}_2[0,\infty)$ denotes any continuous signals on $[0,\infty)$ that possess a finite 2-norm [22]. The following definitions and remarks are presented to prove the stability of the inner loop system.

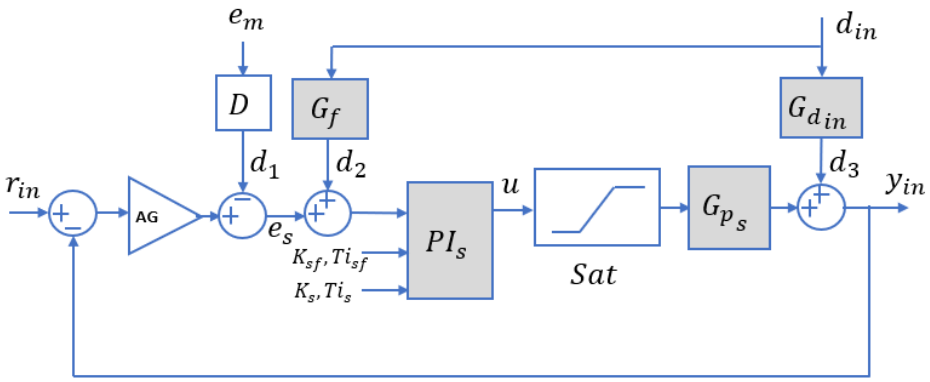

Figure 7. Internal stability of the feedforward-feedback control system.

Definition 1. Assume there is no mismatch between the actual plant and the linear time-invariant (LTI) nominal models. Additionally, assume that the disturbances $d_{in}(t)$ and $e_m(t)$ are bounded. Disturbance rejection is achieved using the feedforward

controller G_f if this controller belongs to the subspace $\mathcal{RH}_\infty$ where $\mathcal{RH}_\infty$ is the real rational subspace of $\mathcal{H}_\infty$ comprising all proper, rational, and stable transfer functions.

Definition 1 emphasizes the fact that feedforward control provides the unique ability to perfectly reject disturbances, a feat that cannot be achieved with feedback control alone. The following analysis aims to assess the performance of feedforward control under realistic conditions where model uncertainties are present.

Definition 2. The system shown in Figure 7 is internally stable if all the transfer functions from the inputs $[r_{in}(t)\ d_{in}(t)\ e_m(t)]^T$ to the outputs $[y_{in}(t)\ u(t)\ d_1(t)\ d_2(t)\ d_3(t)]^T$ belong to the $\mathcal{RH}_\infty$ for all bounded inputs $r_{in}(t), d_{in}(t), e_m(t)$.

Remark 5. For feedforward–feedback internal stability, it is necessary that $G_f(s)$, $G_{d_{in}}(s)$ and $D(s)$ be stable functions. Otherwise, for any bounded $e_m(t)$ and $d_{in}(t) \in \mathcal{L}_2[0,\infty)$, the outputs $d_1(t)$ or $d_2(t)$ or $d_3(t)$ may not be bounded. So, the feedforward–feedback control system in Figure 7 is internally stable if $G_f(s)$ and $G_d(s)$ belong to $\mathcal{RH}_\infty$.

According to Equations (16), (23), and the identified transfer functions for inner loop disturbances ($G_{d1_{in}}$ and $G_{d2_{in}}$ in (1) to (15)), it is observed that the conditions mentioned in Remark 5 are satisfied. Therefore, based on Definition 2 and Remark 5, the feedforward-feedback control system illustrated in Figure 7 is internally stable. However, we would like to further investigate the general conditions under which the feedforward-feedback control system will remain internally stable.

4.1. Robust Stability Conditions for the Feedback-Feedforward Control Loop

Assume we have two nominal models along with their corresponding uncertainty limits to represent the real plant. Consequently, the dynamics of the entire plant can be described using two perturbed models defined through classic multiplicative uncertainty, namely:

$$\begin{aligned} G_{p_{in}}(s) &= G_{p_{in}0}(s)\big(1+\Delta_u(s)\big) \\ G_{d_{in}}(s) &= G_{d_{in}0}(s)\big(1+\Delta_d(s)\big) \end{aligned} \tag{25}$$

where $G_{p_{in}0}(s)$ and $G_{d_{in}0}(s)$ are the nominal models and the uncertainties are limited as follows:

$$\begin{aligned} |\Delta_u(j\omega)| &\le \overline{\Delta}_u(\omega) \\ |\Delta_d(j\omega)| &\le \overline{\Delta}_d(\omega) \end{aligned} \tag{26}$$

where $\overline{\Delta}_u(\omega)$ and $\overline{\Delta}_d(\omega)$ are the upper bounds for the considered uncertainties in plant and disturbance, respectively.

Definition 3. The feedforward–feedback control system has robust stability if the feedback controller $PI_s(s)$ gives internal stability to the closed-loop system for all $G_{p_{in}}(s)$, $G_f(s)$, $D(s)$ and $G_{d_{in}}(s)$ belong to $\mathcal{RH}_\infty$.

According to definition 3, assuming that all $G_{p_{in}}(s)$, $G_f(s)$, $D(s)$ and $G_{d_{in}}(s)$ belong to $\mathcal{RH}_\infty$, the feedback controller $PI_s(s)$ can lead to the stability of the internal closed-loop system with proper tuning. So, the performance of the feedforward–feedback control system can be investigated by the following relation:

$$\frac{y_{in}(s)}{d_{in}(s)} = \frac{G_{d_{in}0}(s)\big(1+\Delta_d(s)\big) + PI_s(s)G_f(s)G_{p_{in}0}(s)\big(1+\Delta_u(s)\big)}{1+\mathrm{AG}\Big(PI_s(s)G_{p_{in}0}(s)\big(1+\Delta_u(s)\big)\Big)} \tag{27}$$

The right side of relation (20) introduces the definition of the closed-loop output resulting from the disturbance signal d_{in}, referred to as $G_{cl_{d_{in}}}(s)$. Therefore, it is evident that the condition:

$$\left|G_{cl_{d_{in}}}(j\omega)\right| \leq \gamma, \qquad \forall\, 0 \leq \omega < \infty \tag{28}$$

ensures:

$$\|y_{in}(j\omega)\| \leq \gamma \|d_{in}(j\omega)\| \tag{29}$$

It is clear from (29) that disturbance attenuation of the output variable is achieved when $\gamma < 1$. This condition indicates that both the feedforward and feedback controllers must be simultaneously tuned to ensure effective disturbance rejection. Then, the following lemma expressed the required condition for robust performance of the feedforward–feedback control system in Figure 7.

Definition 4. The feedforward-feedback control system achieves robust performance if, for every $e_m(t)$ and $d_{in}(t) \in \mathcal{L}_2[0,\infty)$, the desired performance condition is satisfied for every perturbed model $G_{p_{in}}(s)$, and $G_{d_{in}}(s)$. This sufficient condition can be formalized as follows:

$$\left\|\alpha G_{cl_{d_{in}}}\right\|_{\infty} \leq 1 \tag{30}$$

where $|\alpha| = \gamma^{-1} \geq 1$.

Lemma 2. *The feedforward–feedback control system in Figure 7 achieves robust performance if the following condition is satisfied for any perturbed model $G_{p_{in}}(s)$ and $G_{d_{in}}(s)$ that satisfy Equation (26)*:

$$\left|G_{d_{in}0}(j\omega)\left(1+\Delta_d(j\omega)\right) + PI_s(j\omega)G_f(j\omega)G_{p_{in}0}(j\omega)\left(1+\Delta_u(j\omega)\right)\right| + \left|\mathrm{AG}\left(PI_s(j\omega)G_{p_{in}0}(j\omega)\left(1+\Delta_u(j\omega)\right)\right)\right| \leq 1, \qquad \forall\, 0 \leq \omega < \infty \tag{31}$$

Proof. According to Equation (30), we have:

$$\left|\alpha G_{cl_{d_{in}}}(j\omega)\right| \leq 1, \qquad \forall\, 0 \leq \omega < \infty \tag{32}$$

Then, according to Equation (27), we have:

$$\left|\alpha \frac{G_{d_{in}0}(j\omega)\left(1+\Delta_d(j\omega)\right) + G_f(j\omega)G_{p_{in}0}(j\omega)\left(1+\Delta_u(j\omega)\right)PI_s(j\omega)}{1+\mathrm{AG}\left(PI_s(j\omega)G_{p_{in}0}(j\omega)\left(1+\Delta_u(j\omega)\right)\right)}\right| \leq 1\,, \forall\, 0 \leq \omega < \infty \tag{33}$$

Rearranging the above condition gives:

$$\begin{aligned}
&\left|\alpha \frac{G_{d_{in}0}(j\omega)\left(1+\Delta_d(j\omega)\right) + G_f(j\omega)G_{p_{in}0}(j\omega)\left(1+\Delta_u(j\omega)\right)PI_s(j\omega)}{1+\mathrm{AG}\left(PI_s(j\omega)G_{p_{in}0}(j\omega)\left(1+\Delta_u(j\omega)\right)\right)}\right| = \\
&\alpha \frac{\left|G_{d_{in}0}(j\omega)\left(1+\Delta_d(j\omega)\right) + G_f(j\omega)G_{p_{in}0}(j\omega)\left(1+\Delta_u(j\omega)\right)PI_s(j\omega)\right|}{\left|1+\mathrm{AG}\left(PI_s(j\omega)G_{p_{in}0}(j\omega)\left(1+\Delta_u(j\omega)\right)\right)\right|} \leq \\
&\alpha \frac{\left|G_{d_{in}0}(j\omega)\left(1+\Delta_d(j\omega)\right) + G_f(j\omega)G_{p_{in}0}(j\omega)\left(1+\Delta_u(j\omega)\right)PI_s(j\omega)\right|}{1-\left|\mathrm{AG}\left(PI_s(j\omega)G_{p_{in}0}(j\omega)\left(1+\Delta_u(j\omega)\right)\right)\right|}\,, \forall\, 0 \leq \omega < \infty
\end{aligned} \tag{34}$$

From Equation (33) and (34), we have:

$$\alpha \frac{\left|G_{d_{in}0}(j\omega)\left(1+\Delta_d(j\omega)\right) + G_f(j\omega)G_{p_{in}0}(j\omega)\left(1+\Delta_d(j\omega)\right)PI_s(j\omega)\right|}{1-\left|\mathrm{AG}\left(PI_s(j\omega)G_{p_{in}0}(j\omega)\left(1+\Delta_u(j\omega)\right)\right)\right|} \leq 1\,, \forall\, 0 \leq \omega < \infty \tag{35}$$

Rearranging again, we get:

$$\alpha\left|G_{d_{in}0}(j\omega)\left(1+\Delta_d(j\omega)\right)+G_f(j\omega)G_{p_{in}0}(j\omega)\left(1+\Delta_d(j\omega)\right)PI_s(j\omega)\right|+\left|\mathrm{AG}\left(PI_s(j\omega)G_{p_{in}0}(j\omega)\left(1+\Delta_u(j\omega)\right)\right)\right|\leq 1,\qquad \forall\, 0\leq\omega<\infty \tag{36}$$

which is the result in Equation (31).

The stability proof presented above has focused on the analysis of a feedforward-feedback loop for a controller with fixed parameters. However, it is important to note that the inner loop PI controller described in this paper is designed as a gain-scheduling PI controller, where its parameters switch between two values. Additionally, the adaptive gain (AG) also influences the performance of the inner loop. Therefore, in the following section, we will investigate the stability margin for both the adaptive gain and the gain-scheduling PI controller.

4.2. Stability Analysis of Inner Loop Adaptive Gain-Scheduling PI Controller

Based on the structure shown in Figure 7, the characteristic equation of the inner loop closed-loop system is obtained as follows:

$$1+\mathrm{AG}\left(PI_s(s)G_{p_{in}0}(s)\left(1+\Delta_u(s)\right)\right)=0 \tag{37}$$

If we define $G_{p_{in}}(j\omega)=G_{p_{in}0}(j\omega)\left(1+\Delta_u(j\omega)\right)=a(\omega)+jb(\omega)$ in frequency-domain. We have:

$$1+\mathrm{AG}\left(K_s\left(1-\frac{j}{Ti_s\omega}\right)\left(a(\omega)+jb(\omega)\right)\right)=Ti_s\omega+\mathrm{AG}\left(K_s(Ti_s\omega-j)\left(a(\omega)+jb(\omega)\right)\right)=0 \tag{38}$$

The stability region of PI controllers can be analyzed using the D-partition method [23]. According to the D-partition principle, the stability region boundary of the PID controller consists of a singular boundary D at $\omega=0$, $\omega=\pm\infty$, as well as a nonsingular boundary D when $\omega\in(0,-\infty)\cup(0,+\infty)$. Therefore, the results of applying the D-partition principle to Equation (37) are as follows:

- When $\omega=0$, the singular boundary D is

$$\mathrm{AG}.K_s\left(a(\omega)+jb(\omega)\right)=0 \tag{39}$$

- When $\omega=\pm\infty$, the singular value boundary of the PI controller does not exist.
- When $\omega\in(0,-\infty)\cup(0,+\infty)$, the nonsingular boundary values of the PI controller can be determined by setting both the real part and the imaginary part of Equation (38) to zero. This approach yields the boundary values as follows:

$$\begin{cases} Ti_s\omega+\mathrm{AG}.K_s\left(Ti_s\omega\times a(\omega)+b(\omega)\right)=0 \\ \mathrm{AG}.K_s\left(Ti_s\omega\times b(\omega)-a(\omega)\right)=0 \end{cases} \tag{40}$$

In summary, the parameter stability region of the PI controller is as follows:

$$\begin{cases} Ti_s\omega+\mathrm{AG}.K_s\left(Ti_s\omega\times a(\omega)+b(\omega)\right)=0 \\ \mathrm{AG}.K_s\left(Ti_s\omega\times b(\omega)-a(\omega)\right)=0 \\ K_s=0 \\ \mathrm{AG}=0 \end{cases} \tag{41}$$

Therefore, since the polynomials $a(\omega)$ and $b(\omega)$ are known, if the parameters K_s and Ti_s for the PI controller are selected in such a way that Equation (41) is established, the inner loop system will maintain internal stability for every uncertainty in $G_{p_{in}}$. Thus, the switching of parameters K_s and Ti_s in a gain-scheduling PI controller cannot create stability issues in the inner loop as long as the singularity conditions presented in Equation (41) are satisfied. It is also important to note that the adaptive gain (AG) in the y column in Table 3 has been chosen such that Equation (41) is satisfied.

As stated in Lemma 1, to ensure the stability of the entire cascade control system, stability of the inner loop must first be established. Once this is accomplished, the stability of the outer loop can be assured by selecting appropriate PI controller parameters for the

outer loop. Therefore, if the parameters K_s and Ti_s and AG are selected in (34), by choosing an arbitrary frequency ω, the stable interval for the parameters K_m and Ti_m can be obtained by re-applying the principle D-partition on the characteristic equation of the cascade closed-loop system calculated.

The selected parameters for the inner and outer loop PI controllers in section 5 have been selected by applying the Particle Swarm Optimization (PSO) optimization method and considering the obtained stable intervals of the cascade system.

5. Tuning Procedure

In this section, the parameters of the PI and feedforward controllers in Figure 4 are tuned using a tuning method. In the following, the PSO method is used for this purpose. The PSO algorithm is a nature-inspired metaheuristic that aims to find optimal solutions through swarm intelligence. Compared to other numerical optimization methods, such as genetic algorithms, the PSO method offers several advantages, including a faster convergence to optimal parameters, a simpler formulation, and a reduced number of parameters.

5.1. Overview of PSO Algorithm

PSO is an optimization algorithm based on evolutionary computation technique. In PSO, individuals called as particles are evolved by cooperation and competition among themselves through generations. A particle represents a potential solution to a problem. Each particle adjusts its flying according to its own flying experience and its companion flying experience. Each particle is treated as a point in a d-dimensional space. The i-th particle is represented as $x = (x_{i1}, x_{i2}, \dots, x_{id})$. The best previous position (giving the minimum fitness value) of any particle is called p_{best} is presented as $p = (p_{i1}, p_{i2}, \dots, p_{id})$. The index of the best particle among all particles in the population is represented by the symbol g, called as gbest. The velocity for the particle i is represented as $v = (v_{i1}, v_{i2}, \dots, v_{id})$. The particles are updated according to the following equations:

$$v_{id}^{n+1} = w.v_{id}^{n+1} + c_1.rand.(p_{id}^n - x_{id}^n) + c_2.rand.(p_{gd}^n - x_{id}^n) \quad (42)$$

$$x_{id}^{n+1} = x_{id}^n + v_{id}^{n+1} \quad (43)$$

where c_1 and c_2 are two positive constant and are selected as $c_1 = c_2 = 0.5$, $rand()$ is random function between 0 and 1, n represents iteration which in this paper we consider $n = 10$, inertia weight w is brought into the equation to balance between the global search and local search capability and is selected as $w = 0.7$, and finally, d is the swarm size which is usually around 10-50 and in this paper, we set 12. Equation (24) is used to calculate particle's new velocity according to its previous velocity and the distances of its current position from its own best experience (position) (p_{id}^n) and the group's best experience (p_{gd}^n). Then, the particle flies toward a new position according to Equation (25). The performance of each particle is measured according to a pre-defined fitness function (performance index), which is related to the problem to be solved.

5.2. Controller Coefficients Tuning Based on PSO

Different algorithms can be applied for the tuning of PID controller to ensure optimal control performance at nominal operating conditions. In this paper, PSO is employed to tune PI and feedforward controllers' coefficients using measured data and the identified models in Equation (1) to (15). PSO firstly produces initial swarm of particles in search space. Each particle represents a candidate solution for the parameters where their values are set in an appropriate range. According to section 3, several parameters

can be tuned for the structure designed in Figure 4. The parameters considered for tuning in this article are introduced in Table 4.

Table 4. SST control loop tunable parameters.

Parameter	Range
K_m	Gain of Master PI controller
K_s	Gain of Slave PI controller
Ti_m	Time Constant of Master PI controller
Ti_s	Time Constant of Slave PI controller
K_{ffpow}	Power feedforward gain
K_{sf}	Gain of Slave PI controller in drastic changes
K_{ffTfg}	Flue Gas Temperature feedforward gain
Ti_{sf}	Time Constant of Slave PI controller in drastic changes
K_{ffFdb}	Duct burner fuel flow feedforward gain

To optimize the defined nine parameters in Table 4 using PSO, it is necessary to define a suitable performance index. For the SST control loop, the following performance index is considered:

$$PSO\ Performance\ Index = \sum_{i=1}^{n} \left((y_{out}(i) - S.P.)^2 + 0.1 \times \Delta u^2(i) \right) \tag{44}$$

where, the number 0.1 is the coefficient of control effort, which shows the higher importance of minimizing the output error than the control effort in this cost function. Including the control effort term in cost function will reduce control valve fluctuations.

6. Simulation and Implementation Results

In this section, at first, the simulation results for the proposed control structure are presented. Then, the proposed method will be implemented on the SST control loop of two different power plants, Pareh-Sar power plant in Gilan and Parand power plant in Tehran. Since in boilers, the duct burner can be in either the on or off state, and the on or off state of the duct burner has a significant impact on the performance of the SST control loop, the simulations and implementations are presented for both the on and off states of the duct burner. The simulations have been carried out in the Python environment.

6.1. Simulation Results

6.1.1. Controller Coefficients Tuning When the Duct Burner is Off

Before changing the existing SST cascade PI control logic to the proposed feedforward cascade gain-scheduling PI structure, we have done a PSO-based tuning on the inner and outer loop PI controller parameters of the existing control system. The existing and the PSO-tuned PI parameters are presented in the first two rows of the Table 5. Figure 8 shows the steam temperature and control signal (percentage of valve opening) before and after controllers' parameter tuning for a two-hour measured data from Pareh-Sar power plant on 15-April-2023 when the duct burner is off. According to Figure 8, by tuning the parameters of the inner and outer control loops, the amplitude of steady-state fluctuations in steam temperature and water spray control valve has decreased. But it is apparent that it was not able to effectively impact the first peak (overshoot) in steam temperature which is due to a sudden rise in the gas turbine power (MW). In order to solve this problem, the proposed control structure is used.

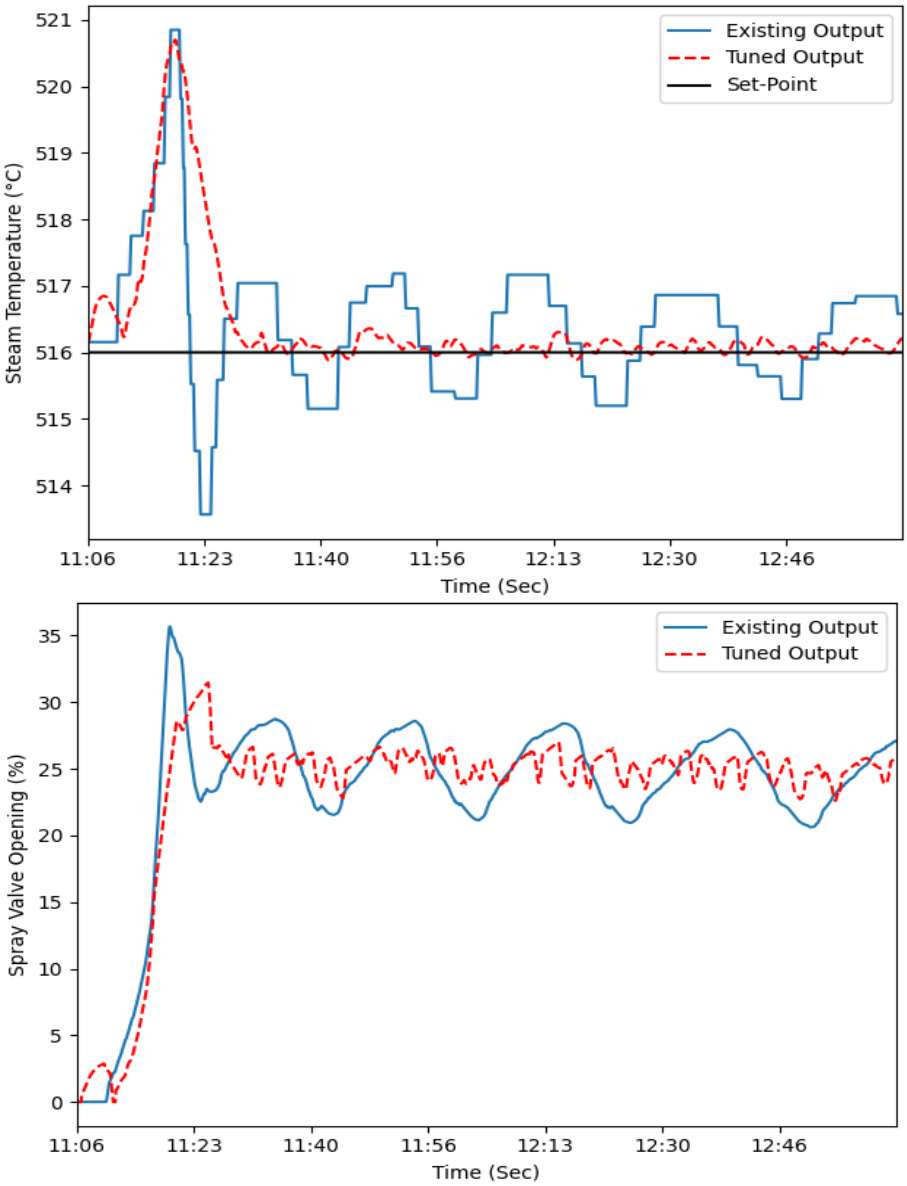

Figure 8. Results of applying tuning using the PSO method for cascade SST control loop for a measured data on 15 April 2023.

In what follows, the results of applying the proposed feedforward gain-scheduling control in algorithm 1 to the same data is presented. The results of tuning the controller parameters using the PSO method for the proposed feedforward gain-scheduling PI cascade control method in this paper can be observed in Table 5. As described in section 3, the gas turbine power (MW) and flue gas temperature (T_{fg}) are used as predictive disturbance signals to inform that there's going to be a rise in steam temperature in advance. Other than the predictive aspect of adding feedforward signal before the feedback controller, the gain-scheduling inner loop PI controller allows the controller to act faster when changes are detected in the gas turbine power (MW) and flue gas temperature (T_{fg}) and to become slower in the steady-state conditions. This helps to reduce the steam temperature initial peak (overshoot) and steady-state fluctuations of both steam temperature and water spray valve.

Table 5. SST control loop tunable parameters.

	K_m	Ti_m	K_s	Ti_s	K_{sf}	Ti_{sf}	K_{ffpow}	K_{fffg}
Existing PI cascade control loop parameters	1	20	1	90	-	-	-	-
PSO-tuned PI cascade control loop parameters	1	110	1.5	150	-	-	-	-
PSO-tuned proposed feedforward gain-scheduling PI cascade control loop parameters	1	110	1	200	1.5	100	30	1.4

According to the Figure 9, it is apparent that the proposed feedforward gain-scheduling control method is able to reduce the steam temperature overshoot by opening the water spray valve earlier. It also reduced the steady-state fluctuations in the steam temperature and water spray valve, since the gain-scheduling structure allows for different steady-state parameter selection. Reducing the steam temperature peak will avoid initiating alarms and trips and thus a higher set-point can be selected for the steam temperature which will result in higher power generation.

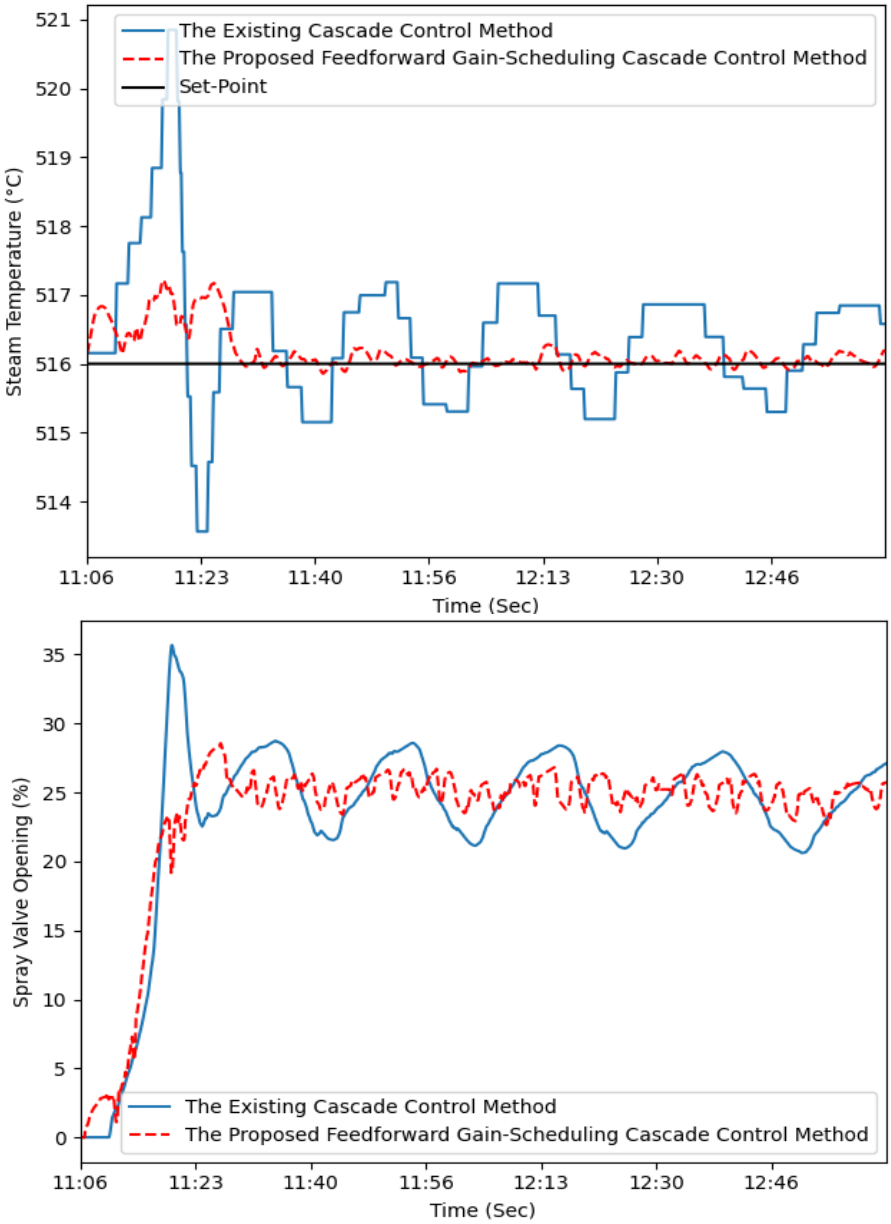

Figure 9. Results of applying the proposed feedforward gain-scheduling control method for the SST control loop for a measured data from Pareh-Sar power plant on 15 April 2023.

Figure 10 shows the result of applying the proposed control structure for 30-April-2023 data in Pareh-Sar power plant, indicating that since there was a noticeable rise in gas turbine load demand on this day, adding feedforward control signals will significantly reduce the steam temperature peak and avoid initiating alarm and trip.

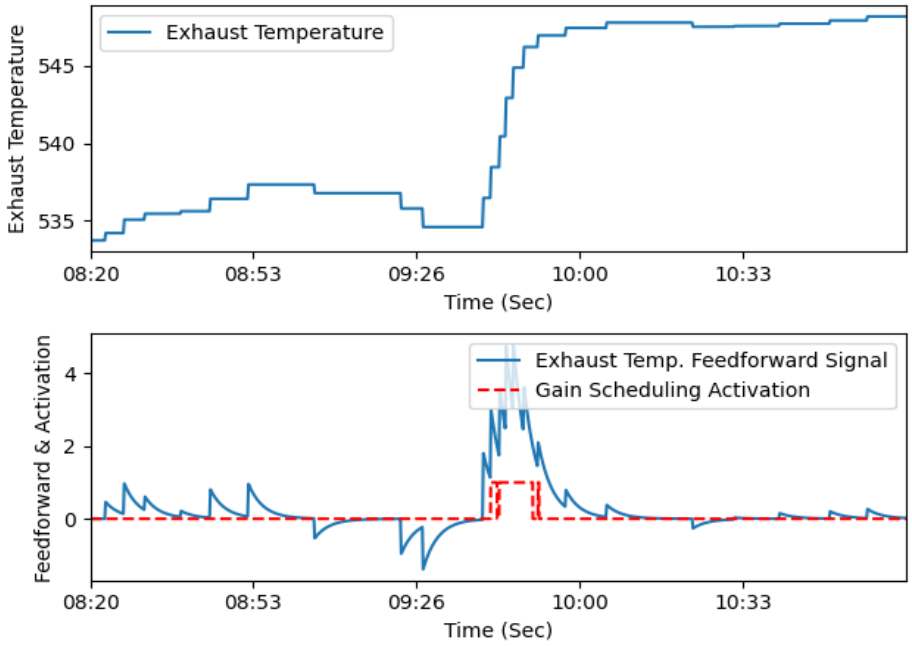

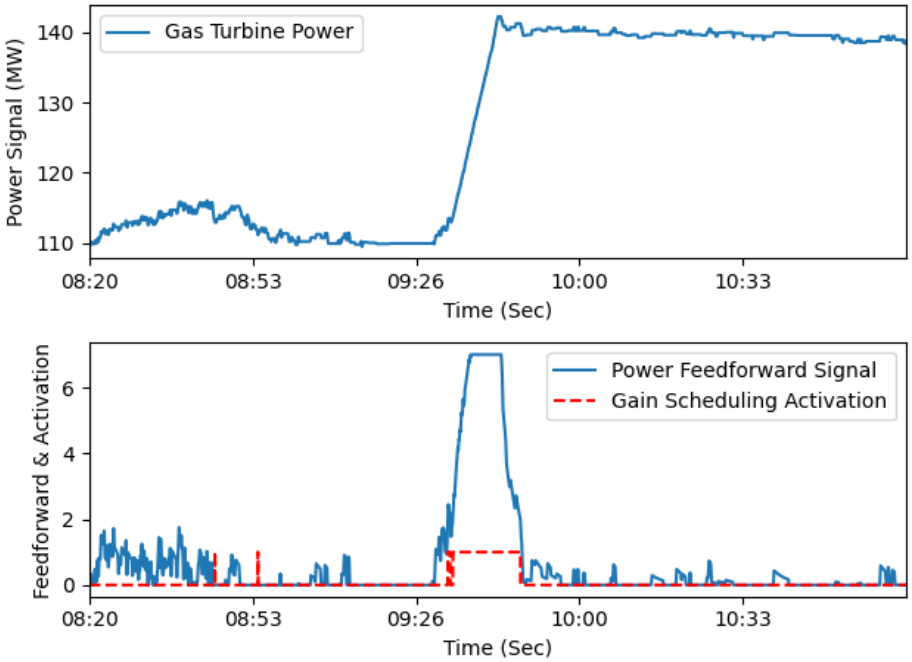

Figure 10. Results of applying the proposed feedforward gain-scheduling control method for the SST control loop for a measured data from Pareh-Sar power plant on 30-April-2023: **(a)** The duct burner fuel flow signal and related gain-scheduling control activation and feedforward signal, **(b)** The gas turbine load signal and related gain-scheduling control activation and feedforward signal, **(c)** steam temperature, and **(d)** spray valve opening.

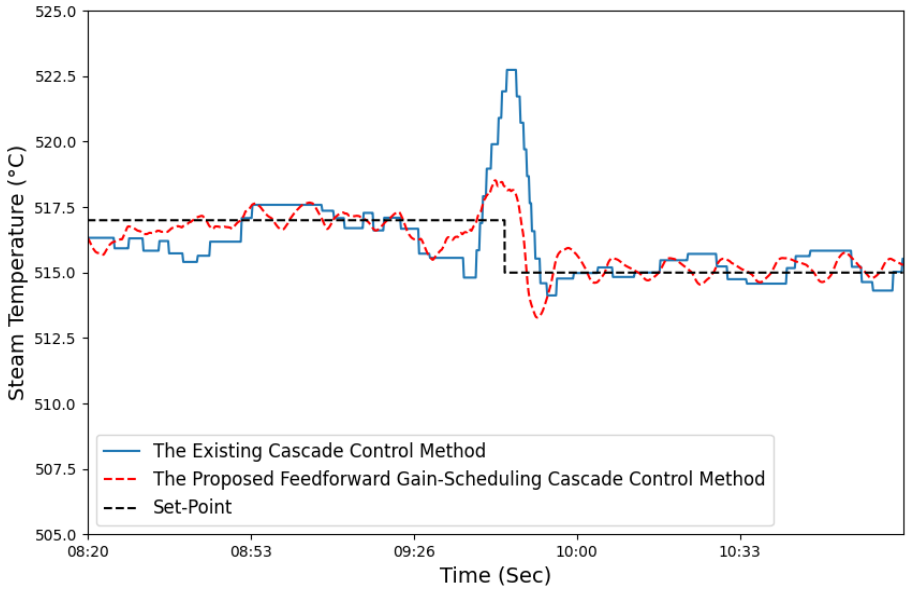

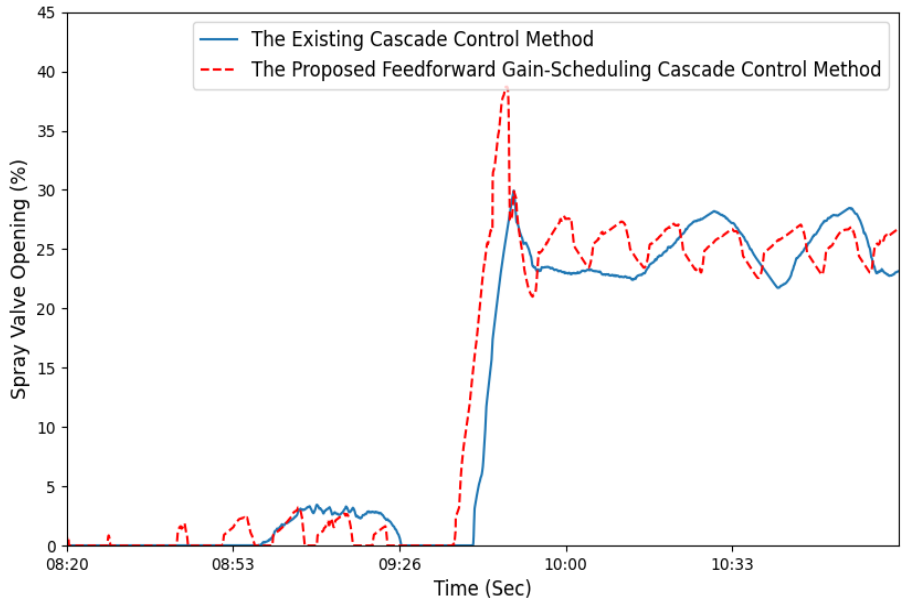

6.1.2. Controller Coefficients Tuning When the Duct Burner is On

As mentioned in Remark 3, when duct burner is on, using the duct burner fuel flow signal as the input of a feedforward signal can lead to an increase in the response speed of the water spray control valve during sudden changes in the duct burner fuel flow (and consequently changes in the HP steam temperature). In this section, while the duct burner is on, the tuning of the proposed structure parameters is addressed. As mentioned, since the duct burners in the Pareh-Sar power plant are always off due to the operating conditions, the measured data from the Parand combined cycle power plant is used to investigate duct burner effect.

Figure 11 shows the result of applying the proposed method for a measured data from Parand power plant SST control loop on 15-June-2024. According to Figure 11 (a) and (b), an increase in the gas turbine power, accordingly, a decrease in the duct burner fuel flow can be observed. In these figures, the feedforward signals made from the power and duct burner flow rate signals as well as the gain-scheduling activation signal are also shown. Whenever the gain-scheduling activation signal becomes 1, the slave PI controller parameters switch to values K_{sf} and Ti_{sf}. The existing and the PSO-tuned PI parameters

are presented in Table 6. Figure 11 also shows the steam temperature and control signal for a one-hour measured data from Parand power plant on 14-June-2024 when the duct burner is on. According to Figure 11, due to the effectiveness of proposed feedforward gain-scheduling control, the spray valve has opened earlier and more than before. This leads to a significant decrease in the temperature peak from 521.5°C to 519.1°C.

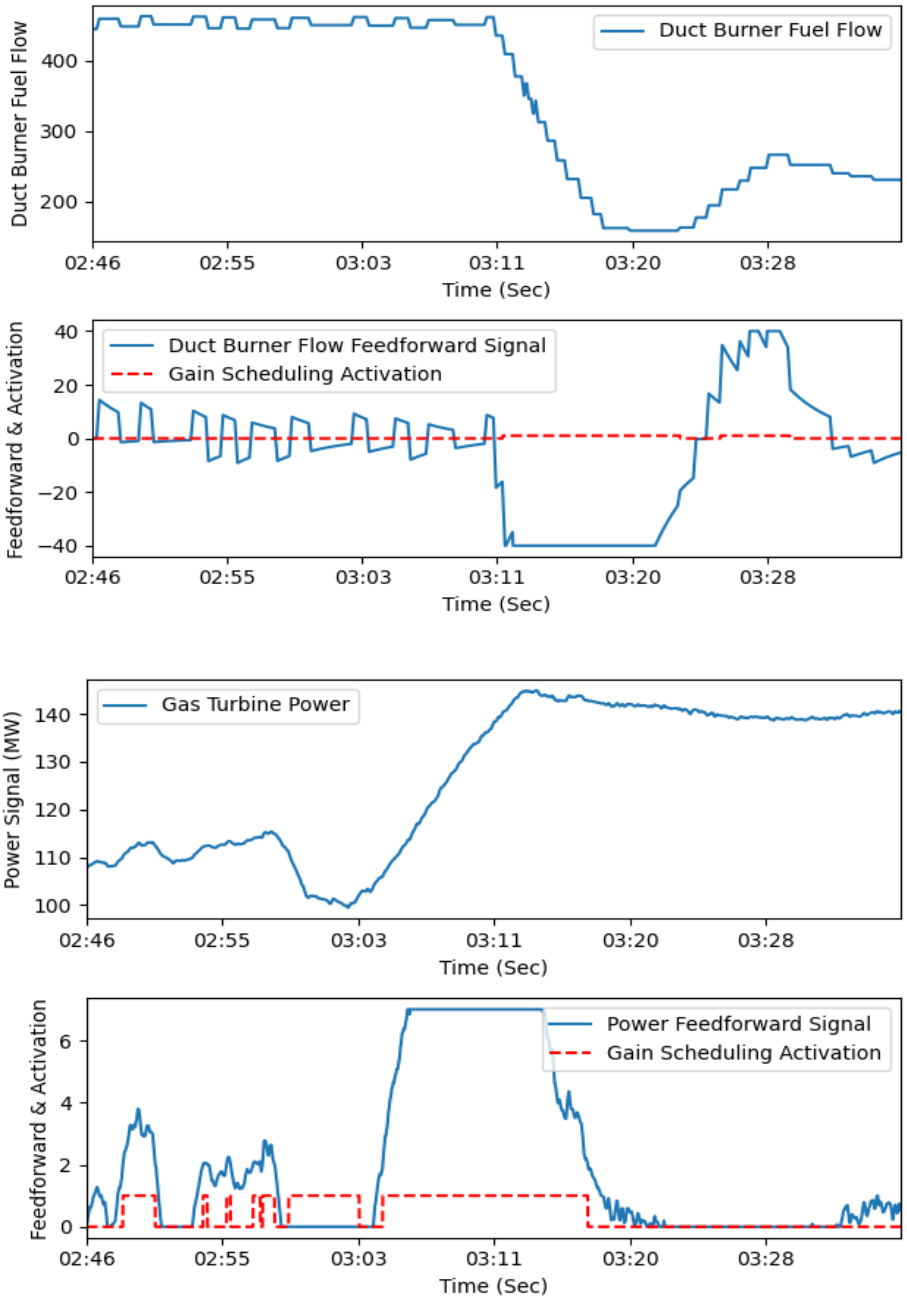

Figure 11. Results of applying the proposed feedforward gain-scheduling control method for the SST control loop for a measured data from Parand power plant on 15-June-2024: **(a)** The duct burner fuel flow signal and related gain-scheduling control activation and feedforward signal, **(b)** The gas turbine load signal and related gain-scheduling control activation and feedforward signal, **(c)** steam temperature, and **(d)** spray valve opening.

(c)

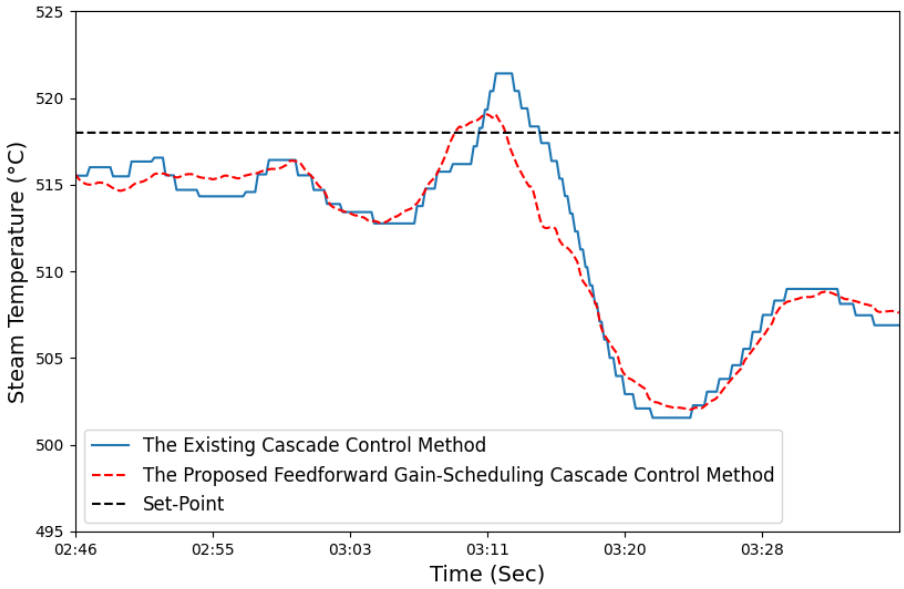

(d)

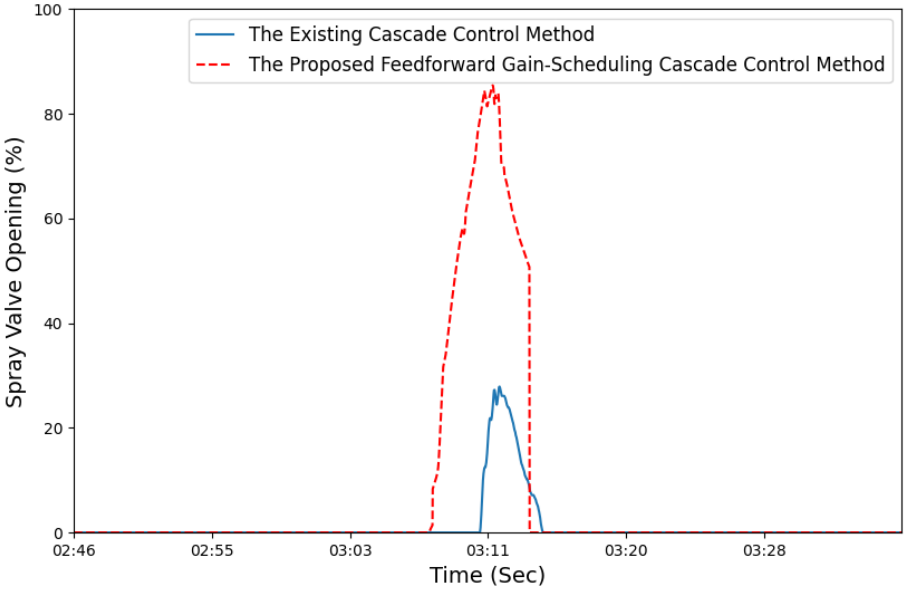

Table 6. Inner and outer PI parameters by applying the proposed method when duct burner is on.

	K_m	Ti_m	K_s	Ti_s	K_{sf}	Ti_{sf}	K_{ffpow}	K_{fftfg}
Existing PI cascade control loop parameters	1	10	1.2	50	-	-	-	-
PSO-tuned proposed feedforward gain-scheduling PI cascade control loop parameters	1.5	120	1.2	150	1.5	100	3	0.3

6.2. Implementation Results

In this section, the results of the practical implementation of the proposed method in this paper are presented for both the cases of the burner duct being on and off, in the Parand and Pareh-Sar power plants, respectively.

6.2.1. Pareh-Sar Power Plant Results

On 15-December-2023, the proposed feedforward gain-scheduling cascade PI control scheme in this paper was implemented for verification on unit 1 HRSG of Pareh-

Sar combined cycle power plant. The results obtained from this implementation are presented in this section.

Currently, the rate of gas turbine power changes in Pareh-Sar power plant is set at 3 megawatts per minute. Therefore, in the first scenario to test the presented control scheme with the change rate 3 megawatts per minute, we examine the spray valve opening and and the steam temperature when the load of the gas turbine increases by about 25 MW. By applying this scenario, the spray valve opening percentage and SST behavior with the proposed control scheme are obtained as presented in Figure 12. According to Figure 12, the maximum steam temperature rise is 1.2°C (516.2°C peak temperature compared to the set-point 515°C), whereas under similar conditions with the previous cascade PI control scheme on 30-April-2023, the SST overshoot was about 6 degrees as presented in Figure 10. As shown in Figure 10, the amount of rise is so high that when the SST reaches 523°C, the corresponding alarm is activated and the operator is forced to reduce the set-point to control the temperature.

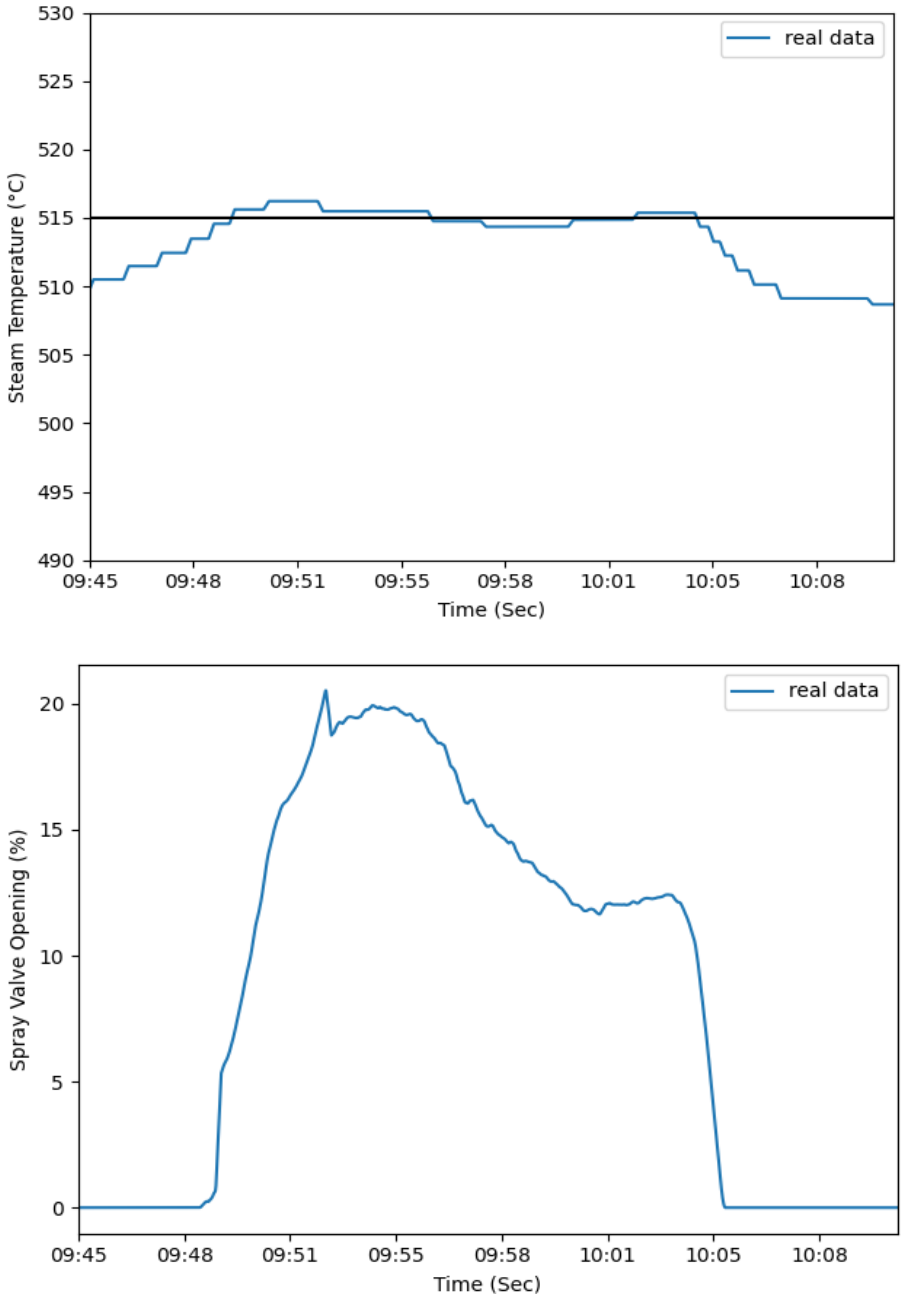

Figure 12. Results of applying the proposed method on the Pareh-Sar superheated HP with 3 megawatts per minute gas turbine power changes rate, on 15 December 2023: **(a)** steam temperature, and **(b)** water spray valve position.

Due to the fact that the increase in gas turbine power may occur at a faster rate, in the second scenario, this rate is set to 6 megawatts per minute and again how the spray valve opens and its effect on the SST when the gas turbine load increment is around 30 megawatts are investigated. In this condition, the SST and the opening percentage of the spray valve are obtained as shown in Figure 13. According to Figure 13, the maximum steam temperature increase is equal to 2.2°C (517.2°C peak temperature compared to the set-point 515°C).

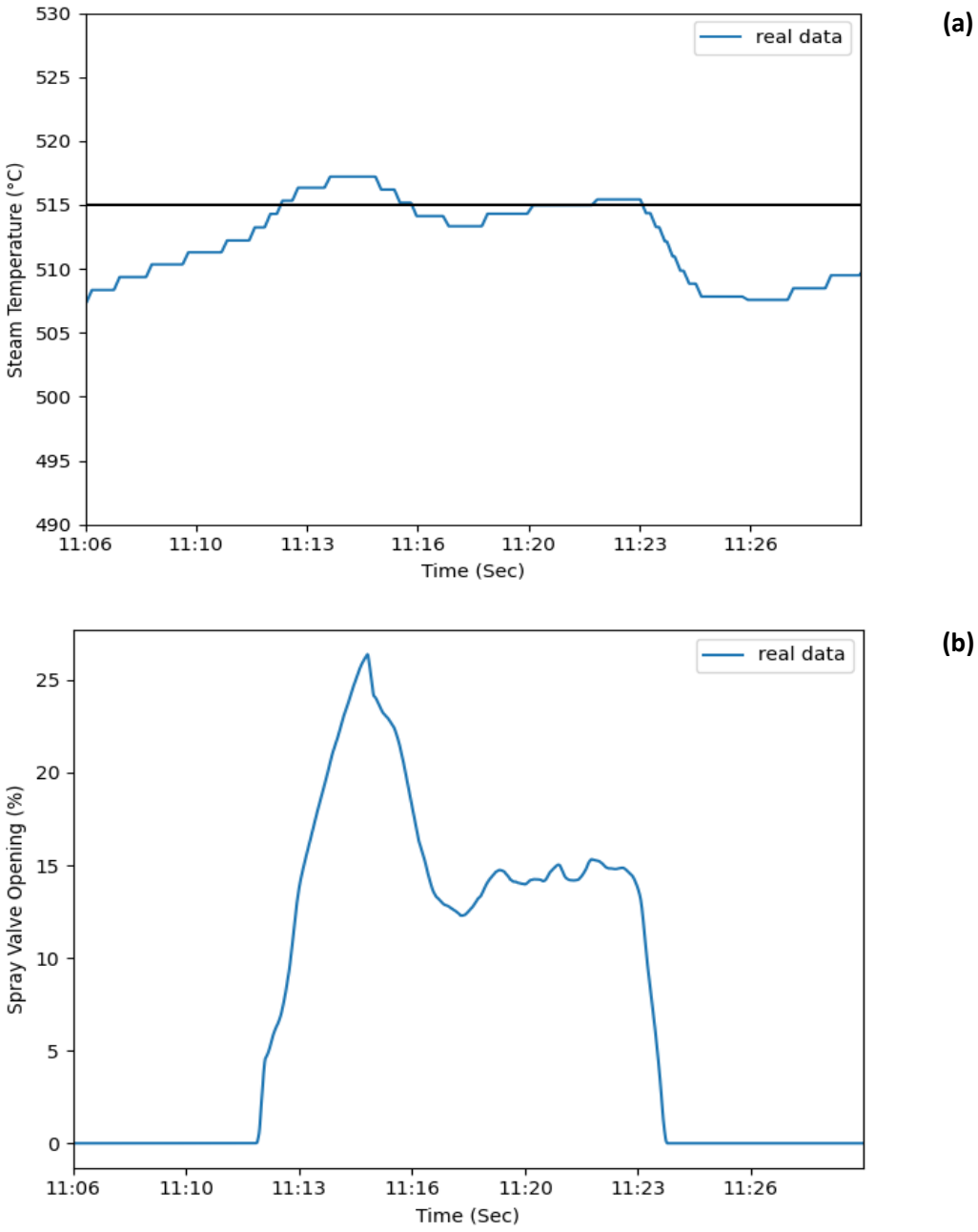

Figure 13. Results of applying the proposed method on the Pareh-Sar superheated HP with 6 megawatts per minute gas turbine power changes rate, on 15 December 2023: **(a)** steam temperature, and **(b)** water spray valve position.

6.2.2. Parand Power Plant Results

On 12-June-2024, the proposed feedforward gain-scheduling cascade PI control scheme in this paper was implemented for verification on unit 4 HRSG of Parand combined cycle power plant. The results are shown in Figure 14. The set-point currently set in the Parand power plant is 518°C. However, to investigate the proposed method, the set-point was changed to 517°C and 516°C during the implementation of the

proposed method. As observed in Figure 14, the temperature fluctuations were adjusted within one degree around the set-point which is an appropriate result.

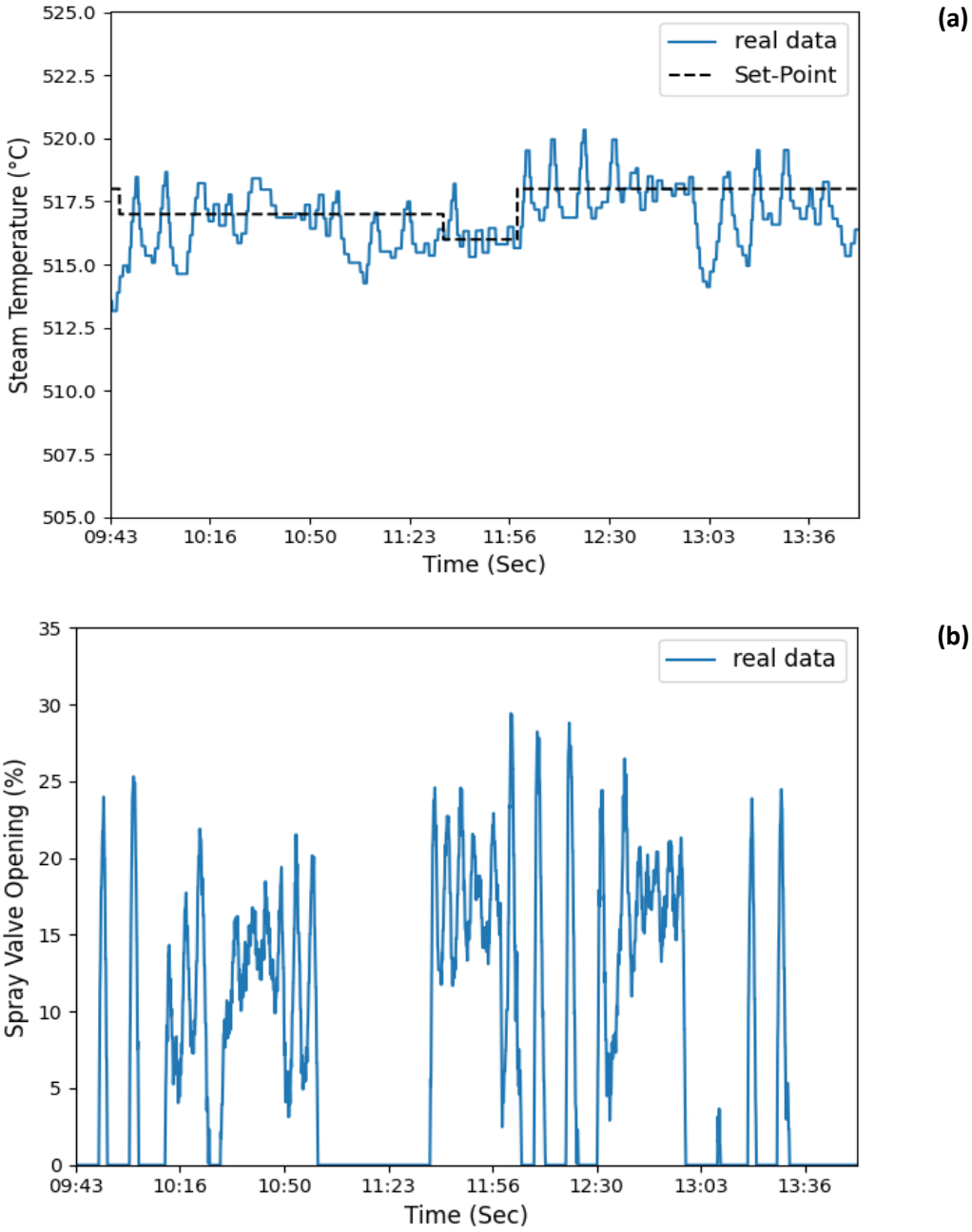

Figure 14. Results of applying the proposed method on the Parand superheated HP, on 12 June 2024: **(a)** steam temperature, and **(b)** water spray valve position.

The proposed control scheme was also implemented on unit 4 HRSG of Parand combined cycle power plant on 23-July-2024. Considering the good results obtained from the set-points 516°C to 518°C, the set-point is increased to a higher value of 521°C in order to increase the production power of the steam turbine. As can be seen in Figure 15, the maximum peak temperature for this set-point is less than 2 degrees. It can be shown that increasing the SST set-point increase can lead to an average increase of 2 MW in the production power of the steam turbine.

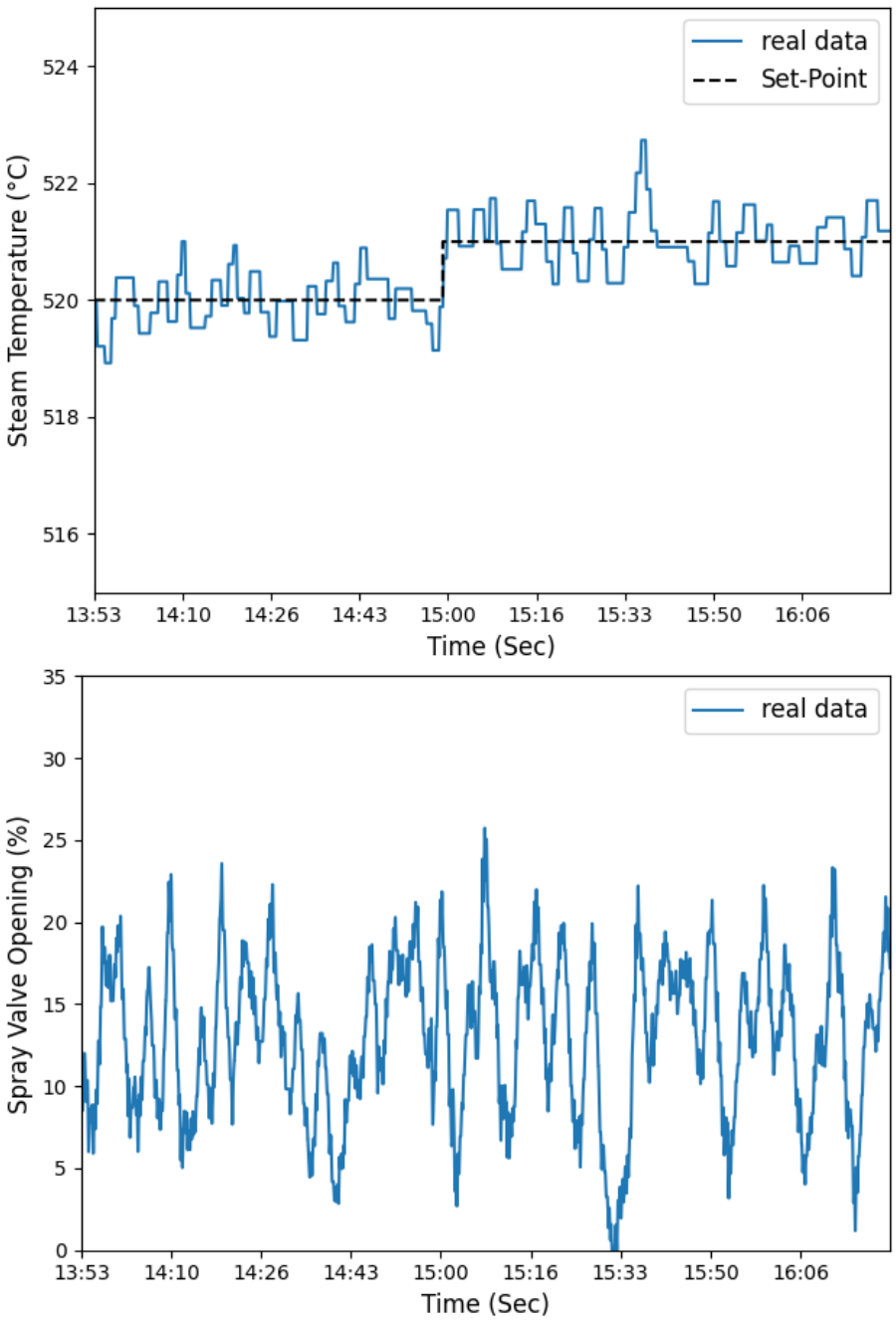

Figure 15. Results of applying the proposed method on the Parand superheated HP, on 12 June 2024: **(a)** steam temperature, and **(b)** water spray valve position.

7. Conclusions

Controlling the temperature of superheated steam is crucial for the safe and economic operation of combined cycle power plants. In this paper, a gain-scheduling PI cascade control strategy along with feed-forward control is presented to effectively control the superheated steam temperature. Due to the use of the defined feedforward controller, the delay between the water spray valve and load and fuel changes is reduced. The results are shown on the models obtained from the system identification, which show the proper performance of the proposed structure in removing disturbances, reducing the fluctuations of tracking set-point and water spray valve position, and significantly reducing temperature overshoot. A theoretical review for stability analysis of the proposed scheme was also presented. Finally, the proposed structure was implemented on the two combined cycle power plants, Pareh-Sar located in Gilan, Iran and Parand

located in Tehran, Iran, which shows 3 to 5 degrees of temperature peak reduction. This reduction in temperature overshoot, will allow for higher SST set-points that will eventually lead to more produced power in a steam cycle. The improvement of SST control in these power plants has been roughly calculated to be able to increase 2 MW in the produced power of each steam turbine.

Funding: This research received no external funding.

Data Availability Statement: The data that support the findings of this study are available from the corresponding author upon reasonable request.

Conflicts of Interest: The authors declare no conflicts of interest.

References

[1] G. Shi, Z. Wu, J. Guo, D. Li, and Y. Ding, "Superheated Steam Temperature Control Based on a Hybrid Active Disturbance Rejection Control," *Energies (Basel)*, vol. 13, no. 7, p. 1757, Apr. 2020, doi: 10.3390/en13071757.

[2] Z. Wu, T. He, D. Li, Y. Xue, L. Sun, and L. Sun, "Superheated steam temperature control based on modified active disturbance rejection control," *Control Eng Pract*, vol. 83, pp. 83–97, Feb. 2019, doi: 10.1016/j.conengprac.2018.09.027.

[3] J. Zhang, F. Zhang, M. Ren, G. Hou, and F. Fang, "Cascade control of superheated steam temperature with neuro-PID controller," *ISA Trans*, vol. 51, no. 6, pp. 778–785, Nov. 2012, doi: 10.1016/j.isatra.2012.06.008.

[4] X.-F. Li, D.-J. Ding, Y.-G. Wang, and Z. Huang, "Cascade IMC-PID Control of Superheated Steam Temperature based on Closed-loop Identification in the Frequency Domain," *IFAC-PapersOnLine*, vol. 49, no. 18, pp. 91–97, 2016, doi: 10.1016/j.ifacol.2016.10.145.

[5] Z. Wu, D. Li, and L. Wang, "Control of the superheated steam temperature: A comparison study between PID and fractional order PID controller," in *2016 35th Chinese Control Conference (CCC)*, IEEE, Jul. 2016, pp. 10521–10526. doi: 10.1109/ChiCC.2016.7555024.

[6] N. Alamoodi and P. Daoutidis, "Nonlinear control of coal-fired steam power plants," *Control Eng Pract*, vol. 60, pp. 63–75, Mar. 2017, doi: 10.1016/j.conengprac.2016.12.005.

[7] Z. Ma, H. Xu, and F. Dong, "Multi Model Robust PID Control of Main Steam Temperature based on Gap Metric," *IOP Conf Ser Earth Environ Sci*, vol. 558, no. 5, p. 052074, Aug. 2020, doi: 10.1088/1755-1315/558/5/052074.

[8] G.-L. Wang, W.-W. Yan, S.-H. Chen, X. Zhang, and H.-H. Shao, "Multivariable constrained predictive control of main steam temperature in ultra-supercritical coal-fired power unit," *Journal of the Energy Institute*, vol. 88, no. 2, pp. 181–187, May 2015, doi: 10.1016/j.joei.2014.06.003.

[9] X. Wu, J. Shen, Y. Li, and K. Y. Lee, "Fuzzy Modeling and Predictive Control of Power plant Steam Temperature System," *IFAC-PapersOnLine*, vol. 48, no. 30, pp. 397–402, 2015, doi: 10.1016/j.ifacol.2015.12.411.

[10] H. Zhu *et al.*, "Modelling and regulation of steam temperatures of a 1000-MW double-reheat boiler with long short-term memory," *IET Control Theory & Applications*, vol. 17, no. 16, pp. 2190–2204, Nov. 2023, doi: 10.1049/cth2.12535.

[11] L. Ma and K. Y. Lee, "Neural network based superheater steam temperature control for a large-scale supercritical boiler unit," in *2011 IEEE Power and Energy Society General Meeting*, IEEE, Jul. 2011, pp. 1–8. doi: 10.1109/PES.2011.6039231.

[12] H. Bushra, O. Fadul-Elmoula, Y. H.-E. Ibrahim, E. M. Hussein, and D. Mahmoud, "Superheated Steam Temperature Control using Fuzzy Logic Controller," *American Scientific Research Journal for Engineering, Technology, and Sciences (ASRJETS)*, vol. 17, no. 1, pp. 34–41, 2016.

[13] X. Liu and X. Kong, "Nonlinear fuzzy model predictive iterative learning control for drum-type boiler–turbine system," *J Process Control*, vol. 23, no. 8, pp. 1023–1040, Sep. 2013, doi: 10.1016/j.jprocont.2013.06.004.

[14] A. Sanchez-Lopez, G. Arroyo-Figueroa, and A. Villavicencio-Ramirez, "Advanced control algorithms for steam temperature regulation of thermal power plants," *International Journal of Electrical Power & Energy Systems*, vol. 26, no. 10, pp. 779–785, Dec. 2004, doi: 10.1016/j.ijepes.2004.08.003.

[15] Xiang-Jie Liu and Ji-Zhen Liu, "Neuro-Fuzzy Generalized Predictive Control of Boiler Steam Temperature," in *2006 6th World Congress on Intelligent Control and Automation*, IEEE, 2006, pp. 6531–6535. doi: 10.1109/WCICA.2006.1714344.

[16] H. Kim, E. K. Kim, J. Kim, K. S. Lee, S. Kim, and Y. Han, "Prediction-based feedforward control of superheated steam temperature of a power plant,"

International Journal of Electrical Power & Energy Systems, vol. 71, pp. 351–357, Oct. 2015, doi: 10.1016/j.ijepes.2015.03.022.

[17] Makeximu, M. Zhu, Y. Sun, Z. Wu, D. Li, and Y. Xue, "Active disturbance rejection control for boiler superheated steam temperature," in *2016 16th International Conference on Control, Automation and Systems (ICCAS)*, IEEE, Oct. 2016, pp. 135–139. doi: 10.1109/ICCAS.2016.7832310.

[18] L. Sun, Q. Hua, J. Shen, Y. Xue, D. Li, and K. Y. Lee, "Multi-objective optimization for advanced superheater steam temperature control in a 300 MW power plant," *Appl Energy*, vol. 208, pp. 592–606, Dec. 2017, doi: 10.1016/j.apenergy.2017.09.095.

[19] T. He, Z. Wu, D. Li, and J. Wang, "A Tuning Method of Active Disturbance Rejection Control for a Class of High-Order Processes," *IEEE Transactions on Industrial Electronics*, vol. 67, no. 4, pp. 3191–3201, Apr. 2020, doi: 10.1109/TIE.2019.2908592.

[20] X. Li and X. Yu, "Robust regulation for superheated steam temperature control based on data-driven feedback compensation," *Appl Energy*, vol. 325, p. 119918, Nov. 2022, doi: 10.1016/j.apenergy.2022.119918.

[21] S. Prasanth, S. Narayanan, N. Sivakumaran, and H. Pratheesh, "The control of superheater steam temperature in power plants using model predictive controller," *Computers and Electrical Engineering*, vol. 115, p. 109109, Apr. 2024, doi: 10.1016/j.compeleceng.2024.109109.

[22] E. J. Adam and J. L. Marchetti, "Designing and tuning robust feedforward controllers," *Comput Chem Eng*, vol. 28, no. 9, pp. 1899–1911, Aug. 2004, doi: 10.1016/j.compchemeng.2004.03.005.

[23] X. Cui *et al.*, "PID Control of a Superheated Steam Temperature System Based on Integral Gain Scheduling," *Energies (Basel)*, vol. 15, no. 23, p. 8978, Nov. 2022, doi: 10.3390/en15238978.